C.1

NACA

RESEARCH MEMORANDUM

THE INTERRELATED EFFECTS OF ENGINE ROTOR MOMENTUM AND FLIGHT REGIME ON THE DYNAMIC STABILITY OF HIGH-PERFORMANCE AIRCRAFT

By Warren J. North

Lewis Flight Propulsion Laboratory
Cleveland, Ohio

NATIONAL ADVISORY COMMITTEE
FOR AERONAUTICS

WASHINGTON

April 17, 1957

NACA RM E57B05

NATIONAL ADVISORY COMMITTEE FOR AERONAUTICS

RESEARCH MEMORANDUM

THE INTERRELATED EFFECTS OF ENGINE ROTOR MOMENTUM AND FLIGHT REGIME ON THE DYNAMIC STABILITY OF HIGH-PERFORMANCE AIRCRAFT[1]

By Warren J. North

SUMMARY

A five-degree-of-freedom analysis of aircraft maneuvering stability showed that gyroscopic moments due to engine rotor momentum produced considerable aircraft rolling asymmetry for certain values of stability derivatives and flight conditions.

Because of its powerful effect on inertia-coupling and effective dihedral, the most important consideration was the initial angle of attack. Critical reductions in dynamic stability were caused by variations of stability derivatives with angle of attack.

At high altitudes and Mach numbers the effective dihedral due to swept wings and large dorsal fin caused oscillations which were either divergent or lightly damped. The periods of oscillations encountered at high altitude are of the same order of magnitude as pilot reaction time. It appears, therefore, that artificial damping must be incorporated in many high-performance aircraft.

INTRODUCTION

The stability of rolling aircraft has become a critical design and operational consideration with the advent of supersonic, high-altitude aircraft. As predicted in reference 1, concentration of weight in the long fuselage and reduced aerodynamic restoring moments at high altitude have caused inertia-coupled rolling divergence in some cases or have increased aircraft yaw and pitch during roll to a point where structural redesign has been required. Flight experiences with roll-coupling are discussed in references 2 and 3. Analog computer studies of transonic rolling stability are given in references 3 and 4.

---

[1]The information presented herein was offered as a thesis in partial fulfillment of the requirements for the degree of Master of Aeronautical Engineering, Princeton University, Princeton, New Jersey, December, 1956.

Since the trend in supersonic aircraft design is toward thin wings of short span, most of the aircraft and fuel weight is concentrated along the fuselage. Therefore, during a rapid rolling maneuver the airplane tends to rotate about its principal longitudinal axis rather than the wind axis. The first 90° of roll translates the initial angle of attack into a sideslip, the magnitude of sideslip depending on Mach number, directional stability, altitude, and rate of roll. The cross-coupling aerodynamic, inertia, and elastic terms then complicate the maneuver and require a theoretical analog which involves all the airplane degrees of freedom.

The ratio of engine thrust to airplane weight is increasing as airplane design speeds increase; turbojet engines designed for very high altitudes will need large cross-sectional areas to handle sufficient mass flow; vertical-takeoff aircraft need large thrust-to-weight ratios and will operate at airspeeds corresponding to near-zero aerodynamic forces and moments. In light of these trends, the engine rotor gyroscopic moment will become a more important dynamic stability parameter, since, in general, the rotor momentum will increase as engines increase in size and thrust.

In references 1, 5, and 6, the assumption of steady rolling was made in order to linearize the equations of motion. Reference 5 extends the theory of reference 1 to show the effect of engine rotor momentum on steady-rolling stability. Reference 6 also extends the theory of reference 1 and demonstrates how the transients in angle of attack and sideslip can be approximated using the steady-rolling assumption. During a supersonic tactical maneuver the rolling velocity will probably be a continual transient since there will be a few instances when it will be necessary to roll rapidly to angles greater than 180°. This report analyzes the transient airplane response during a half-roll maneuver for a wide range of Mach number and shows the effects of variations in engine rotor momentum, Mach number, altitude, static stability, and load factor.

The basic airplane chosen for this theoretical investigation was a supersonic interceptor with highly swept delta wing and tail surfaces.

SYMBOLS

b	wing span, ft
C_D	drag coefficient, drag/q_oS
C_L	lift coefficient, lift/q_oS
C_l	rolling-moment coefficient, rolling moment/q_oSb

C_m	pitching-moment coefficient, $M/q_oS\bar{c}$
C_n	yawing-moment coefficient, N/q_oSb
C_Y	lateral-force coefficient, lateral force/q_oS
$\bar{c}$	wing mean aerodynamic chord, ft
F_Y,F_Z	forces with respect to Y and Z axes, lb
g	acceleration due to gravity, ft/sec^2
I_X,I_Y,I_Z	moments of inertia about X, Y, and Z principal axes, slug-sq ft
I_{X_e}	moment of inertia of engine rotating parts about X axis, slug-sq ft
i_t	stabilizer deflection, deg
i_w	incidence of symmetrical-airfoil wing, deg
L	rolling moment, ft-lb
M	pitching moment, ft-lb
m	mass of airplane, W/g, slug
N	yawing moment, ft-lb
p	rolling velocity, radian/sec
p_c	critical roll rate, radian/sec
p_e	engine rotor angular velocity, radian/sec
q	pitching velocity, radian/sec
q_o	dynamic pressure, lb/sq ft
r	yawing velocity, radian/sec
S	wing area, sq ft
u,v,w	components of velocity V along X, Y, Z principal axes, ft/sec

4394

CU-1 back

[redacted]

V	velocity, ft/sec
W	airplane weight, lb
X,Y,Z	airplane principal axes
α	angle of attack of principal X axis, deg
α_L	$\alpha + \varepsilon$, aerodynamic angle of attack, deg
β	angle of sideslip, deg
δ_a,δ_r	aileron and rudder deflection, respectively, deg
ε	inclination of body axis above positive X axis, deg
θ	Euler elevation angle of positive X axis, deg
ϕ	Euler roll angle, deg
ψ	Euler yaw angle, deg

Superscript:

$\cdot$	derivative with respect to time

Stability derivatives:

$$C_{L_\alpha} = \frac{\partial C_L}{\partial \alpha}$$

$$C_{L_{i_t}} = \frac{\partial C_L}{\partial i_t}$$

$$C_{l_{\delta_a}} = \frac{\partial C_l}{\partial \delta_a}$$

$$C_{l_p} = \frac{\partial C_l}{\partial \frac{pb}{2V}}$$

$$C_{l_r} = \frac{\partial C_l}{\partial \frac{rb}{2V}}$$

[redacted]

$$C_{l_\beta} = \frac{\partial C_l}{\partial \beta}$$

$$C_{m_\alpha} = \frac{\partial C_m}{\partial \alpha}$$

$$C_{m_{i_t}} = \frac{\partial C_m}{\partial i_t}$$

$$C_{m_q} = \frac{\partial C_m}{\partial \frac{qc}{2V}}$$

$$C_{m_{\dot{\alpha}}} = \frac{\partial C_m}{\partial \frac{\dot{\alpha}c}{2V}}$$

$$C_{m_{\beta^2}} = \frac{\partial C_m}{\partial \beta^2}$$

$$C_{n_{\delta_a}} = \frac{\partial C_n}{\partial \delta_a}$$

$$C_{n_{\delta_r}} = \frac{\partial C_n}{\partial \delta_r}$$

$$C_{n_p} = \frac{\partial C_n}{\partial \frac{pb}{2V}}$$

$$C_{n_r} = \frac{\partial C_n}{\partial \frac{rb}{2V}}$$

$$C_{n_\beta} = \frac{\partial C_n}{\partial \beta}$$

$$C_{Y_\beta} = \frac{\partial C_Y}{\partial \beta}$$

$$C_{Y_r} = \frac{\partial C_Y}{\partial \frac{rb}{2V}}$$

[redacted]

PROCEDURE

The motion of a rigid airplane can be completely described by eight differential equations which represent the six degrees of freedom and involve conversion from Euler angular velocities to angular velocities of principal axes. The initial time history of a rolling maneuver can be represented satisfactorily by seven equations if the airplane velocity is assumed nearly constant during these first few seconds of the maneuver. The Mach number will decrease slightly due to the compound effect of greater induced drag and decreased engine thrust associated with inlet flow distortion. However, this Mach number change can be neglected if the airplane is not operating at or just above the transonic range where there is a rapid variation of aerodynamic coefficients with Mach number. The remaining seven equations are derived in appendix A. The equations are written in terms of the principal axes; therefore, the product of inertia terms do not appear in the moment equations.

When the equations of motion are referred to principal axes, airplane drag might be expected to be an important stability consideration, especially at the low lift-drag ratios associated with supersonic flight. Calculations were made with and without the drag terms in the equations for lift and side force. The only significant effect of drag was a slight damping of the extremely large angle-of-attack excursions.

The static stability derivatives for a typical supersonic interceptor were obtained from wind tunnel tests or Mach number extrapolations thereof. Damping derivative components due to the tail surfaces were calculated from static derivatives, whereas wing and fuselage damping components were obtained from theory. Aeroelastic motions were not treated as additional degrees of freedom but in this analysis were considered as fixed corrections to the stability derivatives. Since wind tunnel balances obtain some forces and moments in terms of wind or stability axes, the aerodynamic derivatives were transferred to the principal axes where necessary. Four of the derivatives were considered functions of angle of attack. The stability derivatives and drag coefficients for the basic airplane are shown in table I. Airplane dimensional and mass constants are shown in table II.

The amount of engine rotor momentum used in this analysis was considered to be the maximum for the assumed aircraft size and performance capabilities.

Machine Computation

In the interest of accuracy and in order to include many nonlinear derivatives and functions, the IBM 650 digital computer was used. A picture of the dual machine setup at the NACA Lewis laboratory is shown

in figure 1. The Runge-Kutta method of numerical integration was selected. With an integration step size of 0.04 second, 2 hours of machine time were required to compute and card-punch the time history of a 6-second maneuver. The cards were tabulated and also read into an automatic curve-plotting machine.

Control Input

The aileron deflection was programmed independently as shown in appendix B. Deflection was dependent on roll angle to the extent that roll position determined the point at which aileron neutralization began. For each reference run (zero engine rotor momentum) a trial-and-error procedure was used whereby duration of aileron deflection and amount of reverse aileron were chosen in order to roll to approximately 180° as rapidly as possible.

During the initial stages of the investigation an attempt was made to maintain roll angle with corrective aileron after the desired roll angle was attained. This corrective aileron deflection was attempted using various combinations of roll velocity, roll acceleration, and roll position as controlling parameters. A pilot reaction time of 0.24 second was assumed. The results showed that in most cases this pilot analog was sufficiently out of phase with the maneuver so as to aggravate the error in roll angle. In addition, under extreme angle of attack, effective aileron reversal existed, and the situation was again aggravated when corrective aileron was programmed. Consequently, in order to provide a comparison during left and right rolls in which engine rotor momentum was the only asymmetry, the ailerons were programmed neutral subsequent to the reversal deflection.

Several rolling maneuvers were continued to angles greater than 180° in an attempt to compare divergence tendencies with the steady-roll theory of reference 1.

At the higher values of dynamic pressure, aileron deflection may be limited by large aileron forces and hinge moments. However, for the purpose of this report, momentary full deflection was programmed at all flight conditions.

Although the initial value of stabilizer position was dependent on flight condition, the stabilizer position was maintained constant throughout each maneuver. Zero rudder deflection was maintained for all maneuvers.

RESULTS AND DISCUSSION

Airplane dynamic behavior during rolling maneuvers is complicated by variations of flight parameters and interrelations thereof. Therefore, when discussing the effect of a single parameter such as engine rotor momentum on aircraft dynamic stability, the corresponding flight conditions and stability parameters must be specified.

This report attempts to show first the effects of rotor momentum associated with changes of altitude, Mach number, and initial load factor. Then, for cases where the effect of rotor momentum was most significant, some of the stability parameters were varied in order to determine specific combinations of flight conditions and stability parameters for which the effect of rotor momentum was most critical.

Aeroelastic effects are concealed in Mach number and altitude effects. Figure 2 shows that equal dynamic pressures of 1300 pounds per square foot exist at Mach numbers of 1.7 and 3.5 and altitudes of 30,000 and 60,000 feet, respectively. At this dynamic pressure, reductions of 10 to 60 percent in static stability and control effectiveness are caused by aeroelastic deformation. The effect of aeroelasticity on the stability derivatives can be seen in table I.

Altitude Effects

Half-roll maneuvers were calculated for altitudes of 30,000 and 60,000 feet at a common Mach number of 1.5. The initial load factor was 1 g. The maneuver time histories at 30,000 feet are shown for left roll without rotor momentum and for left and right rolls with rotor momentum in figures 3, 4, and 5, respectively. There was little variation in maximum angle of attack or sideslip for variations in rotor momentum. The maximum excursion in angle of attack was $3\frac{1}{2}^{\circ}$, and maximum sideslip was $-2\frac{1}{2}^{\circ}$. At 60,000 feet (fig. 6) a half-roll maneuver caused a maximum excursion in angle of attack of 8.8° and sideslip of -6.8°. Left roll (fig. 7) with engine momentum resulted in slightly higher values of angle of attack and sideslip, while right roll (fig. 8) was accompanied by slightly lower values. Similar engine effect trends would be expected from the steady-roll theory of reference 5. Although the engine momentum had a small effect on the maneuver at both altitudes, the variation was somewhat greater at the higher altitude. Since the magnitude of maximum roll rate was 4.5 radians per second at the lower altitude as compared with 1.6 at the higher altitude, it appears that the roll rate had lesser effect on angle of attack and sideslip than did altitude. The altitude effect was largely due to reduction of dynamic pressure which caused an increase in initial inclination of the

principal axis from 3° to 9.3°. The reduction of roll rate with increased altitude is due to reduction in dynamic pressure, reduction in aileron effectiveness at high angles of attack, and strong dihedral effect (positive rolling moment due to negative sideslip). In fact, at the higher altitude (fig. 6) the magnitude of rolling velocity decreased to zero at 2 seconds although full aileron was applied. Note also that angle of attack had increased to 13° and angle of sideslip was negative. Since dihedral effect also increases with angle of attack for a swept midwing configuration, increasing angle of attack has a compound effect on reduction of rolling velocity.

4394

Mach Number Effects

The effect of supersonic Mach number on a half-roll maneuver can be determined by comparing figures 6 (Mach number, 1.5) and 9 (Mach number, 3.5). Both figures represent 60,000 feet and level flight. At the higher Mach number the aircraft responded much more rapidly to aileron input since angle of attack was small and dynamic pressure was high. The small excursions in angles of attack and sideslip at the higher Mach number are due to small initial inclination of the principal axis and large restoring moments. Although the excursions of angles of attack and sideslip were smaller at Mach number 3.5, the increments of normal and lateral accelerations were greater because of a five-fold increase in dynamic pressure. At 1 second, during the high-speed maneuver, the angle of attack and corresponding airplane normal acceleration became negative. The negative acceleration sensed by the pilot would be augmented by a negative increment because of his position above the roll axis. From the pilot's viewpoint this negative acceleration, coupled with the higher normal and lateral accelerations, would make the high-speed maneuver less tolerable.

CU-2

It is interesting to note that the period of oscillation in sideslip is essentially the same at both Mach numbers. This is probably due to the reduction in directional stability at the higher Mach number. The inclusion of engine rotor momentum had no significant effect on the maneuver at Mach number 3.5.

Initial Load Factor

From the standpoint of inertia-coupling, variation of initial load factor is synonymous with variation of the principal axis inclination. Figures 10, 9, and 11 show calculated half-roll maneuvers at a Mach number of 3.5 and an altitude of 60,000 feet for initial load factors of 0, 1, and 2, respectively. The corresponding initial inclinations of the principal axis were 1°, 4°, and 7.3°. At zero g initial condition (fig. 10), the maximum roll velocity exceeded 5 radians per second

magnitude, but primarily because the principal axis was essentially alined with the flight path during the maneuver, there was little variation in angles of attack and sideslip as the airplane rolled. The absence of yawing moment due to aileron deflection aided in permitting this extremely stable rolling condition. At 1 g initial condition (fig. 9) it has been observed previously that there was a moderate oscillation, but the variation in angles of attack and sideslip were within allowable limits. At 2 g initial condition (fig. 11) large oscillations are noted in sideslip and roll, which were triggered by inertia-coupling and maintained by strong effective dihedral coupling. Angle of attack increased beyond the allowable value corresponding to 7 g maximum airplane load factor. Figures 12 and 13 present left- and and right-roll maneuvers at 2 g's with the engine rotor momentum included. It can be noted that variations in angles of attack and sideslip are increased slightly in left rolls and retarded in right rolls.

Increased load factor was not as critical at lower dynamic pressures. At low pressures an increase in load factor required large angles of attack. At high angles of attack the effective dihedral counteracted much of the aileron rolling moment so that high roll rates became more difficult to attain.

Effective Dihedral C_{l_β}

It has been previously noted that the basic airplane configuration exhibited strong positive dihedral effect. Figure 14 shows a half-roll maneuver with zero effective dihedral at a Mach number of 1.5 and an altitude of 60,000 feet. Zero engine rotor momentum was assumed during this maneuver. Zero effective dihedral might be realized with a low straight-wing installation incorporating a ventral fin in addition to the conventional dorsal fin. Negative wing dihedral would also tend to offset the yaw-induced rolling moment due to dorsal fin or angle of attack. As noted in figure 14, the initial angle of attack was translated into negative sideslip during the first 90° of roll. Positive directional stability would normally decrease sideslip, but the combined effect of inertia-coupling and decreasing directional stability caused the motion to diverge in sideslip, reaching -30° at 3.9 seconds. The directional stability decreased because of increasing angle of attack. Figures 15 and 16 show left and right rolls with the inclusion of rotor momentum. If the airplane equations of motion are analyzed, it can be noted that the following engine rotor momentum terms are added to the pitch and yaw equations, respectively:

$$-\frac{I_{X_e} p_e}{I_Y} r; \qquad \frac{I_{X_e} p_e}{I_Z} q$$

[redacted]

At time subsequent to 2.4 seconds (fig. 15) the positive pitching velocity causes an engine-induced positive yawing moment which accelerated the divergence in sideslip. The sideslip reached a magnitude of 30° in 3.5 seconds in this left-roll maneuver. During the right roll (fig. 16) different phase relations are found between pitching and yawing velocities. As a consequence, the rotor couple differs from that for the left roll and tends to stabilize the maneuver. Although not as pronounced, similar dynamic tendencies were found at a Mach number of 0.85 and an altitude of 30,000 feet when the dihedral effect was zero. In comparing figure 14 with figure 6, the omission of effective dihedral uncouples the aerodynamic forces such that rolling velocity is not impeded and also has a destabilizing effect, since sideslip is not bled off in roll. Aircraft stabilization due to positive effective dihedral is shown in figure 11. This run represents a Mach number of 3.5 for which directional stability was very low and decreased to zero at an angle of attack of 7°. Although the angle of attack during a majority of the run was greater than 7°, the airplane did not diverge in sideslip but developed a Dutch-roll-type oscillation with coupling in roll and sideslip.

4394

CU-2 back

Static Stability C_{m_α}, $C_{m_{\beta 2}}$, and C_{n_β}

An important drag consideration for aircraft which operate over a wide range of Mach numbers is the large trim drag due to high longitudinal stability at low supersonic Mach numbers. In-flight reduction of longitudinal stability would therefore be desirable. One way of reducing longitudinal stability in flight would be by fuel transfer. Figure 17 shows the airplane response to aileron roll in level flight at a Mach number of 1.5 and an altitude of 60,000 feet with longitudinal stability reduced by a factor of 10. By comparing figures 17 and 6 the initial effect of the reduced stability is seen to reduce the angle of attack to lower values during the initial roll transient. The lower angle of attack permitted greater aileron effectiveness, which created a faster roll and a sharper recovery. The subsequent coupling in roll and yaw caused a severe slowly damped oscillation. Angle of attack slowly diverged during the maneuver reaching 33° at 6 seconds. Note that the period of the small superimposed oscillation in angle of attack was one-half that in yaw and roll. The periods of the oscillations decreased considerably during this brief maneuver. The slow divergence in angle of attack was, in part, due to the increase in pitching moment with sideslip $C_{m_{\beta 2}}$. Figure 18 shows that the omission of $C_{m_{\beta 2}}$ stabilizes the maneuver.

Reference 1 indicates that for steady-rolling maneuvers the critical roll rates above which the aircraft would exhibit divergence in angles of

[redacted]

attack or sideslip can be calculated. These critical roll rates are the natural frequencies of the independent longitudinal and lateral modes. However, reference 1 shows that an aircraft should never diverge in a steady-rolling maneuver if the critical roll rates in pitch and yaw are identical. The permissible difference between the two critical rates is shown to increase with damping in pitch and yaw. The critical roll rates for the basic configuration are shown in table III. Since directional stability was dependent on angle of attack, the value of directional stability used in these critical roll calculations corresponded to the steady-state angle of attack prior to aileron deflection. For the original stability levels used in figures 7 and 8, level flight, a Mach number of 1.5, and an altitude of 60,000 feet, the corresponding critical roll rates in pitch are -1.68 and 1.80 radians per second, respectively, for left and right rolls with rotor momentum. The critical roll rates in pitch and yaw are nearly equal. Although peak roll rates slightly exceed the calculated critical values for the reference airplane, average roll rates were considerably lower and the convergent oscillation might have been anticipated from steady-rolling divergence theory. The critical roll rates in pitch were reduced to -0.53 and 0.57 radian per second when longitudinal stability was reduced by a factor of 10 (figs. 19 and 20). The maximum roll rates during the initial roll exceed the critical rates by a factor of four, yet this portion of the maneuver did not exhibit a divergence. The slow divergence in angle of attack occurred afted the aileron was neutralized.

Figures 21, 22, and 23 show airplane behavior when both directional and longitudinal stability were reduced to low values. The pitching and yawing critical roll velocities were chosen equal. Again the roll rate during the initial portion of the run exceeded the critical rates by a factor of four. Recovery from the roll caused divergent oscillations in yaw and pitch and a divergent increase in angle of attack. The divergence was more severe than that associated with unequal static stabilities. The effects of rotor momentum were small but similar to previously mentioned trends.

Roll Velocity

Figures 24, 25, and 26 show the time histories of rolling maneuvers in which aileron deflection was maintained until high rates of roll were realized. These runs were made at a Mach number of 3.5 and an altitude of 60,000 feet. The initial values of normal acceleration were the same as those of the previous section Initial Load Factor. It is noted that for zero g (figs. 10 and 24) there is little variation in angles of attack and sideslip for roll rates of 5 and 10 radians per second. At 1 g initial acceleration (figs. 9 and 25) the variation in angles of

[redacted]

attack and sideslip increased slightly as maximum roll rate increased from 5.2 to 9.5 radians per second. At 2 g initial acceleration (figs. 11 and 26) the amplitude of angles of attack and sideslip increased to divergence as roll velocity was increased from a magnitude of 4.3 to 8.4 radians per second but then became stable as roll velocity was increased to 12.5. Apparently the extremely high rolling velocity had a spin-stabilizing effect on the airplane. It is also noted in figure 26 that the largest variations in angles of attack and sideslip occurred after the aileron was neutralized. In every case mentioned previously the maximum roll rate exceeded the critical roll rate. Although the calculated critical values may be used as an approximate criteria for divergence, it appears that, for the transient-type rolling maneuver considered herein, initial inclination of the principal longitudinal axis will be the important consideration.

Comparison with Simplified Longitudinal- and Lateral-Mode Theory

The independent longitudinal and lateral modes were calculated by the linear small-disturbance theory. All stability derivatives were assumed constant and were based on angle of attack at the beginning of the maneuver. The independent modes can be compared with the computed motions subsequent to the half roll when the ailerons were returned to neutral.

The longitudinal equations consisted of only the lift and pitch equations since airplane velocity was assumed constant. The resulting quadratic equation might be expected to give two imaginary roots representing a short-period oscillation. However, for all the flight conditions itemized in table I, the longitudinal quadratic gave two real roots representing two aperiodic modes, one with a fast convergence and one with a weak convergence. The five-degree-of-freedom analysis for Mach number 3.5 (fig. 11) showed a slow oscillation in angle of attack with a faster oscillation superimposed. The oscillations were probably due to the inertia- and aerodynamic-coupling caused by rolling velocity. These disturbing forces were neglected in the linear solution for the longitudinal mode.

Calculations of the lateral mode were made for two Mach number conditions at an altitude of 60,000 feet. The linearized side force, roll, and yaw equations were combined to form a quartic from which four roots were extracted. For each of the two cases investigated the quartic yielded two real roots and two imaginary roots. In each case, the real roots represented a slow divergence and a slow convergence. At Mach number 1.5 the imaginary roots indicate an oscillation with a 4-second period which damps to half-amplitude in $2\frac{1}{2}$ seconds. At Mach number 3.5 the lateral-mode theory predicts a period of 8 seconds which is damped

[redacted]

to half-amplitude in 1 second. At Mach numbers of 1.5 and 3.5 (figs. 6 and 11) the five-degree-of-freedom analysis shows periods which are smaller by factors of 3 and 8, respectively. The actual damping of the oscillations varies during the maneuver considered. The divergences in some of the motions would not be predicted by linear theory, because the destabilizing parameters such as initial inclination of principal axis, nonlinear derivatives, and inertia-coupling are not considered in the linearized theory.

Because of the many simplifications which are made in the linear theory, it is not surprising that there is poor agreement between this and the machine-computed results. This disagreement stresses the need for at least five-degree-of-freedom calculations when computing the transient dynamics of high-altitude, high-performance aircraft.

CONCLUDING REMARKS

A theoretical analysis of dynamic stability for high-performance aircraft showed that several combinations of flight parameters caused divergence or large oscillations in angles of attack and sideslip as a result of a half-roll maneuver. The initial inclination of the principal longitudinal axis was the most critical consideration. There were no roll-induced oscillations when the initial load factor was zero, that is, when the principal longitudinal axis was nearly alined with the flight path.

In one supersonic right-roll maneuver at low dynamic pressure the addition of engine rotor momentum caused gyroscopic moments sufficient to stabilize a divergence. However, inclusion of the rotor momentum during left roll aggravated the divergence. The corresponding airplane configuration possessed zero effective dihedral. This is an important stability consideration because low values of effective dihedral may be prevalent in future supersonic airplanes. The addition of a ventral fin, negative wing dihedral, or the incorporation of a straight wing would reduce airplane effective dihedral. The use of a ventral fin may be required to offset the decrease in supersonic directional stability associated with the dorsal fin at increasing angles of attack.

For most configurations and flight regimes investigated the inclusion of engine rotor momentum caused larger oscillations during left roll than during right roll. This asymmetric roll response will require different pilot techniques dependent on roll direction.

An important consideration when computing dynamic stability is the variation of stability derivatives with angle of attack. Increasing angle of attack can cause reductions or reversals in aileron effectiveness, yaw due to roll, and directional stability. It also has a

powerful effect on swept-wing effective dihedral. These angle-of-attack effects can cause dynamic instability and variations in frequency of the oscillatory motions.

When using electronic computers to compute aircraft maneuvering stability, divergences and oscillations should be assessed in terms of pilot controllability. As in the cases of the classical phugoid and spiral modes, which were often divergent but controllable, some of the supersonic roll-coupled instabilities may be controllable. For the airplane configuration considered herein, the fast lateral oscillations, primarily of the Dutch-roll type, would be difficult to control. However, the large angles of attack usually resulted from slower pitching motions which would be easier to control. Assuming that pitch control was feasible, the angle of attack should not become excessive and the amplitudes of the angle-of-attack-dependent lateral motions should be reduced. Since the critical motions occurred after recovery from the initial roll, pilot judgment and control would not be affected by the radial acceleration associated with rapid rolling, which occurs during the initial portion of the maneuver.

From the standpoint of pilot technique, maneuvering divergences and oscillations can be decreased by performing the roll portion of the maneuver at reduced load factor. This technique may retard slightly the desired change in flight path direction. However, in the case of an interceptor, the absence of subsequent roll-coupled oscillations would permit a more stable gun or missile-launching platform. The above procedure would not be applicable if the principal longitudinal axis were considerably below the body axis.

The incorporation of large positive effective dihedral caused severe roll-and-yaw coupled oscillations which were either divergent or lightly damped. Since the periods of the oscillations were of the same order of magnitude as pilot reaction time, it appears that artificial damping must be incorporated on many high-altitude, high-speed aircraft.

Poor correlation of results with simplified linear longitudinal- and lateral-mode theory stresses the need for at least five-degree-of-freedom calculations when computing the transient dynamics of high-altitude, high-performance aircraft.

Lewis Flight Propulsion Laboratory
National Advisory Committee for Aeronautics
Cleveland, Ohio, February 11, 1957

[redacted]

APPENDIX A

DERIVATION OF EQUATIONS

Principal Axis System

The relation of the airplane axes with the velocity and gravity vectors is shown in the following sketch:

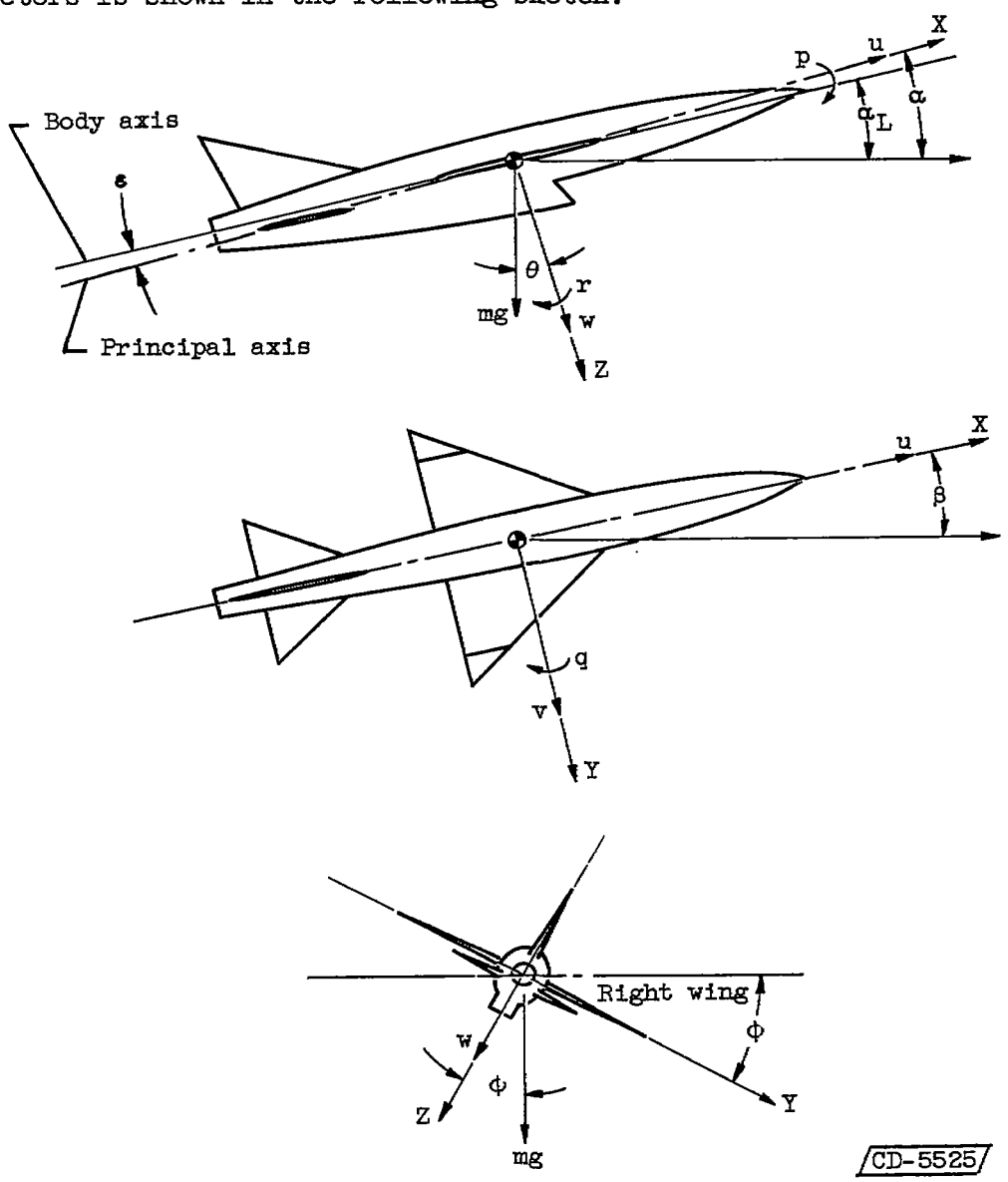

(a)

Equations of Motion

Velocity components:

$$u = V \cos \alpha \cos \beta$$

$$v = V \sin \beta \qquad \dot{v} = V\dot{\beta} \cos \beta$$

$$w = V \sin \alpha \qquad \dot{w} = V\dot{\alpha} \cos \alpha$$

Lift equation:

$$F_{Z_{inertia}} = -m(\dot{w} - uq + vp)$$

$$= -mV\dot{\alpha} \cos \alpha + mVq \cos \alpha \cos \beta - mVp \sin \beta$$

$$F_{Z_{gravity}} = mg \cos \theta \cos \phi$$

$$F_{Z_{aero}} = -C_L q_o S \cos \alpha - C_{L_{i_t}} q_o S \cos \alpha - C_D q_o S \sin \alpha$$

Equating $\Sigma F_Z = 0$ and solving for $\dot{\alpha}$:

$$\dot{\alpha} = q \cos \beta - p \frac{\sin \beta}{\cos \alpha} + \frac{g}{V} \frac{\cos \theta \cos \phi}{\cos \alpha} - \frac{q_o S}{mV} C_{L_\alpha} \alpha_L - \frac{q_o S}{mV} C_{L_{i_t}} i_t - C_D \frac{q_o S}{mV} \frac{\sin \alpha}{\cos \alpha} \tag{A1}$$

Side force:

$$F_{Y_{inertia}} = -m(\dot{v} - wp + ur)$$

$$= -mV\dot{\beta} \cos \beta + mVp \sin \alpha - mVr \cos \alpha \cos \beta$$

$$F_{Y_{gravity}} = mg \sin \phi \cos \theta$$

$$F_{Y_{aero}} = q_o S C_{Y_\beta} \beta + q_o S \frac{b}{2V} C_{Y_r} r - C_D q_o S \sin \beta$$

$$\therefore \dot{\beta} = p \frac{\sin \alpha}{\cos \beta} - r \cos \alpha + \frac{g}{V} \frac{\sin \phi \cos \theta}{\cos \beta} - C_D \frac{q_o S}{mV} \frac{\sin \beta}{\cos \beta} +$$

$$\frac{q_o S}{mV} \frac{C_{Y_\beta} \beta}{\cos \beta} + \frac{q_o S b}{2mV^2} C_{Y_r} \frac{r}{\cos \beta} \tag{A2}$$

[redacted]

Rolling moment:

$$L_{inertia} = -\dot{p}I_X + qr(I_Y - I_Z)$$

$$L_{aero} = q_o SbC_{l_{\delta_a}}\delta_a + \frac{q_o Sb^2}{2V}C_{l_p}p + \frac{q_o Sb^2}{2V}C_{l_r}r + q_o SbC_{l_\beta}\beta$$

$$\therefore \dot{p} = \frac{I_Y - I_Z}{I_X}qr + \frac{q_o Sb}{I_X}C_{l_{\delta_a}}\delta_a + \frac{q_o Sb^2}{2VI_X}C_{l_p}p + \frac{q_o Sb^2}{2VI_X}C_{l_r}r + \frac{q_o Sb}{I_X}C_{l_\beta}\beta \tag{A3}$$

Pitching moment:

$$M_{inertia} = -\dot{q}I_Y + pr(I_Z - I_X) - I_{X_e}p_e r$$

$$M_{aero} = q_o S\bar{c}C_{m_\alpha}\alpha_L + q_o S\bar{c}C_{m_{i_t}}i_t + \frac{q_o S\bar{c}^2}{2V}C_{m_q}q + \frac{q_o S\bar{c}^2}{2V}C_{m_{\dot{\alpha}}}\dot{\alpha} + q_o S\bar{c}C_{m_{\beta^2}}\beta^2$$

$$\therefore \dot{q} = \frac{I_Z - I_X}{I_Y}pr - \frac{I_{X_e}p_e}{I_Y}r + \frac{q_o S\bar{c}}{I_Y}C_{m_\alpha}\alpha_L + \frac{q_o S\bar{c}}{I_Y}C_{m_{i_t}}i_t +$$

$$\frac{q_o S\bar{c}^2}{2VI_Y}C_{m_q}q + \frac{q_o S\bar{c}^2}{2VI_Y}C_{m_{\dot{\alpha}}}\dot{\alpha} + \frac{q_o S\bar{c}}{I_Y}C_{m_{\beta^2}}\beta^2 \tag{A4}$$

Yawing moment:

$$N_{inertia} = -\dot{r}I_Z + (I_X - I_Y)pq + I_{X_e}p_e q$$

$$N_{aero} = q_o SbC_{n_\beta}\beta + \frac{q_o Sb^2}{2V}C_{n_r}r + \frac{q_o Sb^2}{2V}C_{n_p}p + q_o SbC_{n_{\delta_a}}\delta_a + qSbC_{n_{\delta_r}}\delta_r$$

$$\therefore \dot{r} = \frac{I_X - I_Y}{I_Z}pq + \frac{I_{X_e}p_e}{I_Z}q + \frac{q_o Sb}{I_Z}C_{n_\beta}\beta + \frac{q_o Sb^2}{2VI_Z}C_{n_r}r +$$

$$\frac{q_o Sb^2}{2VI_Z}C_{n_p}p + \frac{q_o Sb}{I_Z}C_{n_{\delta_a}}\delta_a + \frac{q_o Sb}{I_Z}C_{n_{\delta_r}}\delta_r \tag{A5}$$

Conversion of Angular Velocities from Principal to Euler Axes

The order of rotation of the axis system is shown in the following sketch:

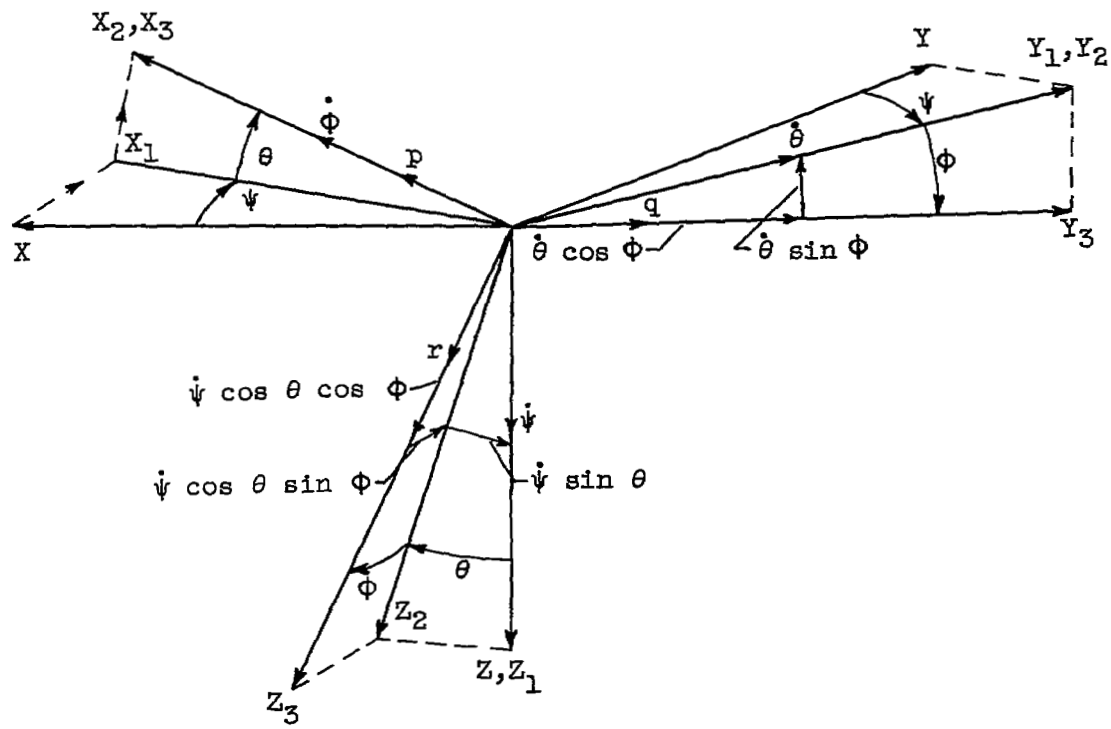

In order to keep the gravity force properly oriented during a maneuver, the relation between the velocities of the Eulerian and principal body axes must be determined. If an airplane is assumed initially in level flight and then is displaced arbitrarily, the displacement can be considered a succession of three rotational velocities:

(1) Rotation $\dot{\psi}$ about Z axis

(2) Rotation $\dot{\theta}$ about Y axis

(3) Rotation $\dot{\Phi}$ about X axis

[redacted]

The resultant body angular velocity vectors p, q, and r are then considered orthogonal. The body rotational velocities can be written in terms of the nonorthogonal Eulerian rotational velocities as follows:

$$p = \dot{\phi} - \dot{\psi} \sin \theta$$

$$q = \dot{\theta} \cos \phi + \dot{\psi} \sin \phi \cos \theta$$

$$r = \dot{\psi} \cos \phi \cos \theta - \dot{\theta} \sin \phi$$

A simultaneous solution of the above three equations yields the Eulerian angular velocities in terms of the body angular velocities:

$$\dot{\phi} = p + q \tan \theta \sin \phi + r \cos \phi \tan \theta \tag{A6}$$

$$\dot{\theta} = q \cos \phi - r \sin \phi \tag{A7}$$

$$\dot{\psi} = r \frac{\cos \phi}{\cos \theta} + q \frac{\sin \phi}{\cos \theta}$$

Only equations (A6) and (A7) are required to describe the change in Eulerian angles which affect the gravitational force, gravity being independent of airplane directional sense.

In addition to the five differential equations of motion, equations (A6) and (A7) were also included in the set which was solved on the computer.

[redacted]

APPENDIX B

AILERON SCHEDULE

The rate of total aileron deflection was chosen as 100° per second with ±28° as maximum deflection:

$$\dot{\delta}_a = \pm 100,\ 0 \text{ (depending on } \Phi,\ \delta_a) \qquad \text{(B1)}$$

A sample left-roll aileron schedule is illustrated in the following sketch:

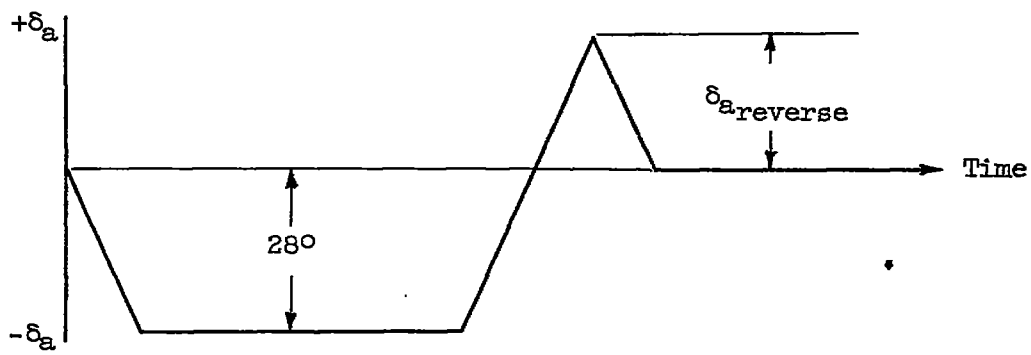

REFERENCES

1. Phillips, William H.: Effect of Steady Rolling on Longitudinal and Directional Stability. NACA TN 1627, 1948.

2. NACA High-Speed Flight Station: Flight Experience with Two High-Speed Airplanes Having Violent Lateral-Longitudinal Coupling in Aileron Rolls. NACA RM H55A13, 1955.

3. Stone, Ralph W., Jr.: Some Notes on the Violent Lateral-Longitudinal Coupling Motions of the Douglas X-3 Airplane in Aileron Rolls. NACA RM L56C15, 1956.

4. Weil, Joseph, and Day, Richard E.: An Analog Study of the Relative Importance of Various Factors Affecting Roll Coupling. NACA RM H56A06, 1956.

5. Gates, Ordway B., Jr., and Woodling, C. H.: A Theoretical Analysis of the Effect of Engine Angular Momentum on Longitudinal and Directional Stability in Steady Rolling Maneuvers. NACA RM L55G05, 1955.

6. Sternfield, Leonard: A Simplified Method for Approximating the Transient Motion in Angles of Attack and Sideslip During a Constant Rolling Maneuver. NACA RM L56F04, 1956.

[redacted]

TABLE I. - STABILITY DERIVATIVES AND DRAG COEFFICIENTS

Altitude, ft	30,000		60,000	
Mach number	0.85	1.5	1.5	3.5
C_{L_α} per deg	0.056	0.0419	0.0508	0.0225
$C_{L_{i_t}}$ per deg	0.0087	0.00508	0.0060	0.00286
C_{m_α} per deg	-0.00645	-0.00846	-0.0124	-0.001536
$C_{m_{i_t}}$ per deg	-0.01413	-0.00916	-0.0109	-0.00527
C_{m_q} per rad	-4.17	-2.78	-3.22	-1.45
$C_{m_{\dot{\alpha}}}$ per rad	-1.69	-0.498	-0.715	-0.557
$C_{m_{\beta 2}}$ per deg^2	0.00033	0.00033	0.00033	0.00025
C_{Y_β} per deg	-0.0202	-0.01665	-0.01955	-0.01176
C_{Y_r} per rad	1.03	1.08	1.08	0.32
C_{l_p} per rad	-0.208	-0.110	-0.1732	-0.0585
C_{l_r} per rad	0.185	0.117	0.117	0.061
C_{n_r} per rad	-0.885	-0.925	-0.925	-0.350
$C_{n_{\delta_a}}$ per deg	0	0	0	0
C_{l_β} per deg	$-0.0029 - 0.00008\ \alpha_L$	$-0.00275 - 0.00015\ \alpha_L$	$-0.00275 - 0.00015\ \alpha_L$	$-0.0008 - 0.00002\ \alpha_L$
$C_{l_{\delta_a}}$ per deg	$0.001042 - 0.302\times10^{-5}\ \alpha_L^2$	$0.000472 - 0.12\times10^{-5}\ \alpha_L^2$	$0.00085 - 0.216\times10^{-5}\ \alpha_L^2$	$0.0003 - 0.294\times10^{-6}\ \alpha_L^2$
C_{n_p} per rad	$0.045 - 0.0138\ \alpha_L$	$0.0303 - 0.0128\ \alpha_L$	$0.0356 - 0.0151\ \alpha_L$	$0.0292 - 0.0063\ \alpha_L$
C_{n_β} per deg	$0.00635 - 0.207\times10^{-4}\ \alpha_L^2$ ($\alpha_L > 0$)	$0.00459 - 0.141\times10^{-4}\ \alpha_L^2$ ($\alpha_L > 0$)	$0.0054 - 0.166\times10^{-4}\ \alpha_L^2$ ($\alpha_L > 0$)	$0.001 - 0.00015\ \alpha_L$
C_D	$0.0155 + 0.000488\ \alpha_L^2$	$0.024 + 0.000415\ \alpha_L^2$	$0.024 + 0.000582\ \alpha_L^2$	$0.020 + 0.000358\ \alpha_L^2$

4394

[redacted]

TABLE II. - AIRPLANE CONSTANTS

S, sq ft	401
m, slug	1,087
b, ft	35.8
$\bar{c}$, ft	15
ε, deg	-1
i_w, deg	0
I_X, slug-sq ft	11,000
I_Y, slug-sq ft	345,000
I_Z, slug-sq ft	344,000
$I_{X_e}p_e$, slug-sq ft/sec	40,000

TABLE III. - CRITICAL ROLL RATES

$$\text{Yaw:}\quad p_c = \pm\left(\frac{C_{n_\beta} q_o S b}{I_Y - I_X}\right)^{\frac{1}{2}} + \frac{I_{X_e} p_e}{2(I_Y - I_X)}$$

$$\text{Pitch:}\quad p_c = \pm\left(\frac{-C_{m_\alpha} q_o S \bar{c}}{I_Z - I_X}\right)^{\frac{1}{2}} + \frac{I_{X_e} p_e}{2(I_Z - I_X)}$$

Mach number	Altitude, $ft \times 10^{-3}$	Initial load factor	Critical roll rate, radian/sec			
			Yaw		Pitch	
			Right	Left	Right	Left
0.85	30	1	2.18	-2.07	1.52	-1.40
.85	30	2	1.83	-1.71	1.52	-1.40
1.5	30	1	3.37	-3.25	3.00	-2.88
1.5	30	2	3.29	-3.18	3.00	-2.88
1.5	60	1	1.64	-1.52	1.80	-1.68
1.5	60	2	.65	-.53	1.80	-1.68
3.5	60	1	1.37	-1.25	1.50	-1.38
3.5	60	2	.53	-.41	1.50	-1.38

[redacted]

Figure 1. - Digital computer arrangement.

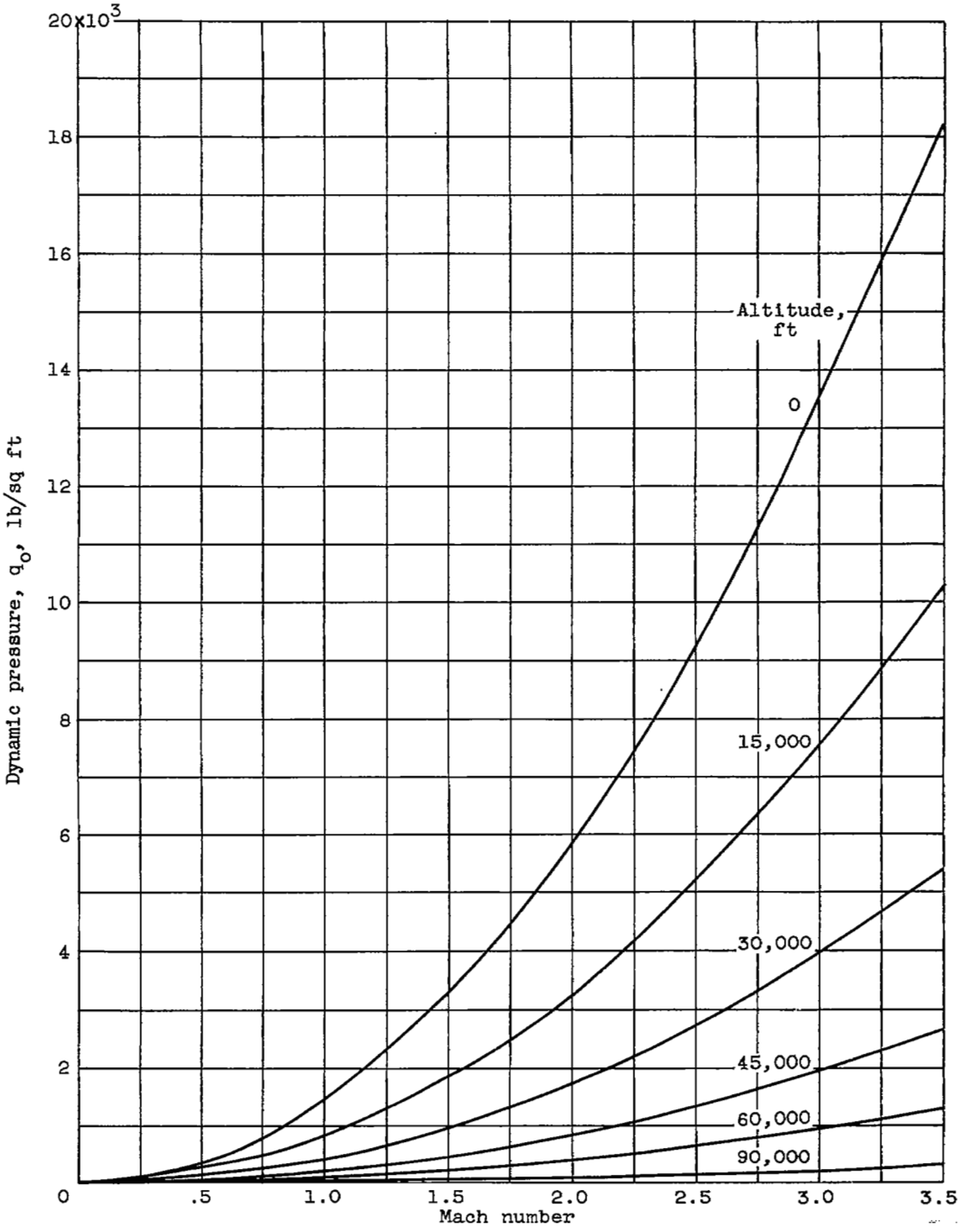

Figure 2. - Variation of dynamic pressure with Mach number and altitude.

[redacted]

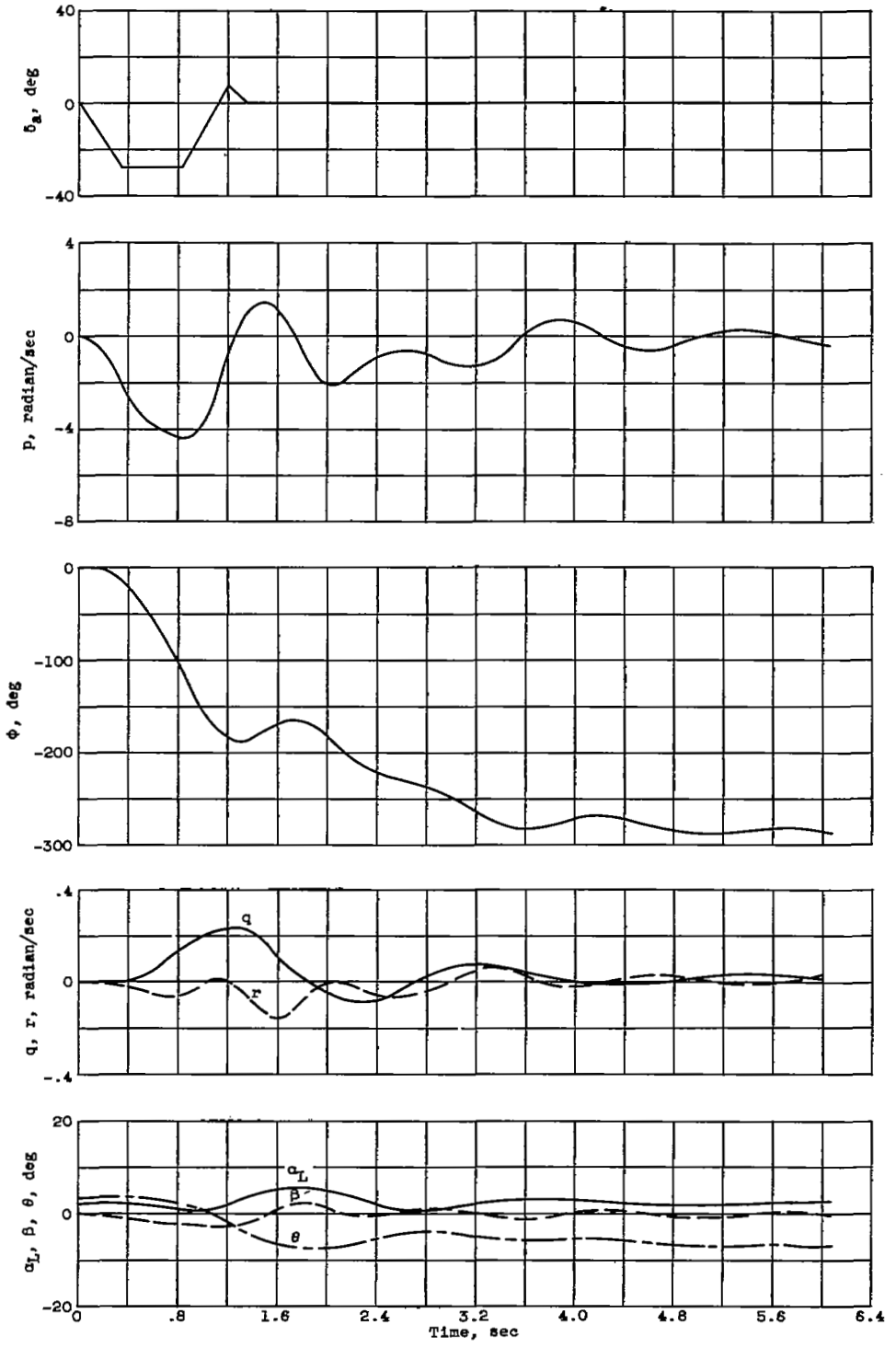

Figure 3. - Left-roll maneuver at Mach number of 1.5, altitude of 30,000 feet, and level flight.

[redacted]

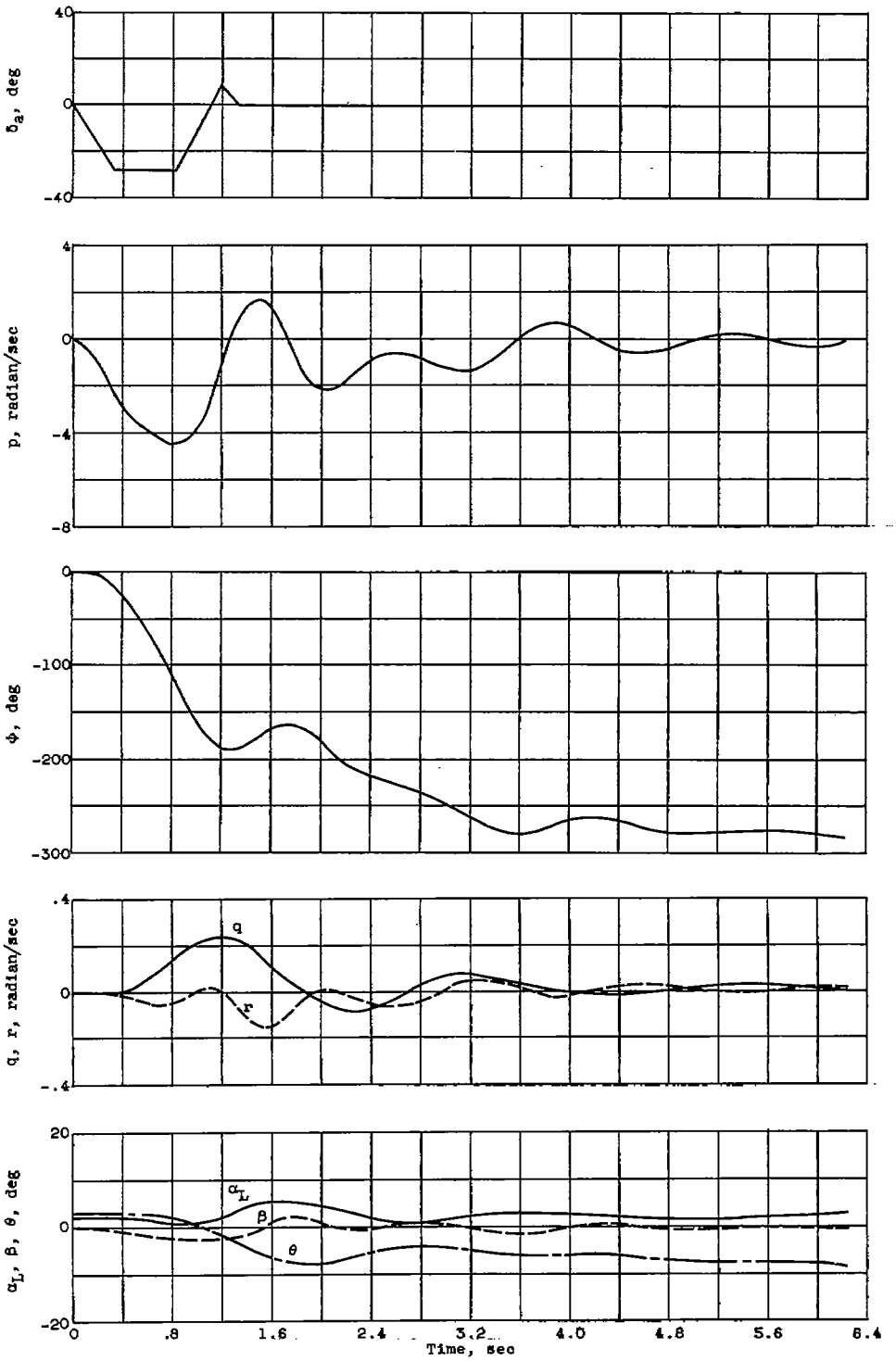

Figure 4. - Left-roll maneuver at Mach number of 1.5, altitude of 30,000 feet, and level flight. Rotor momentum included.

[redacted]

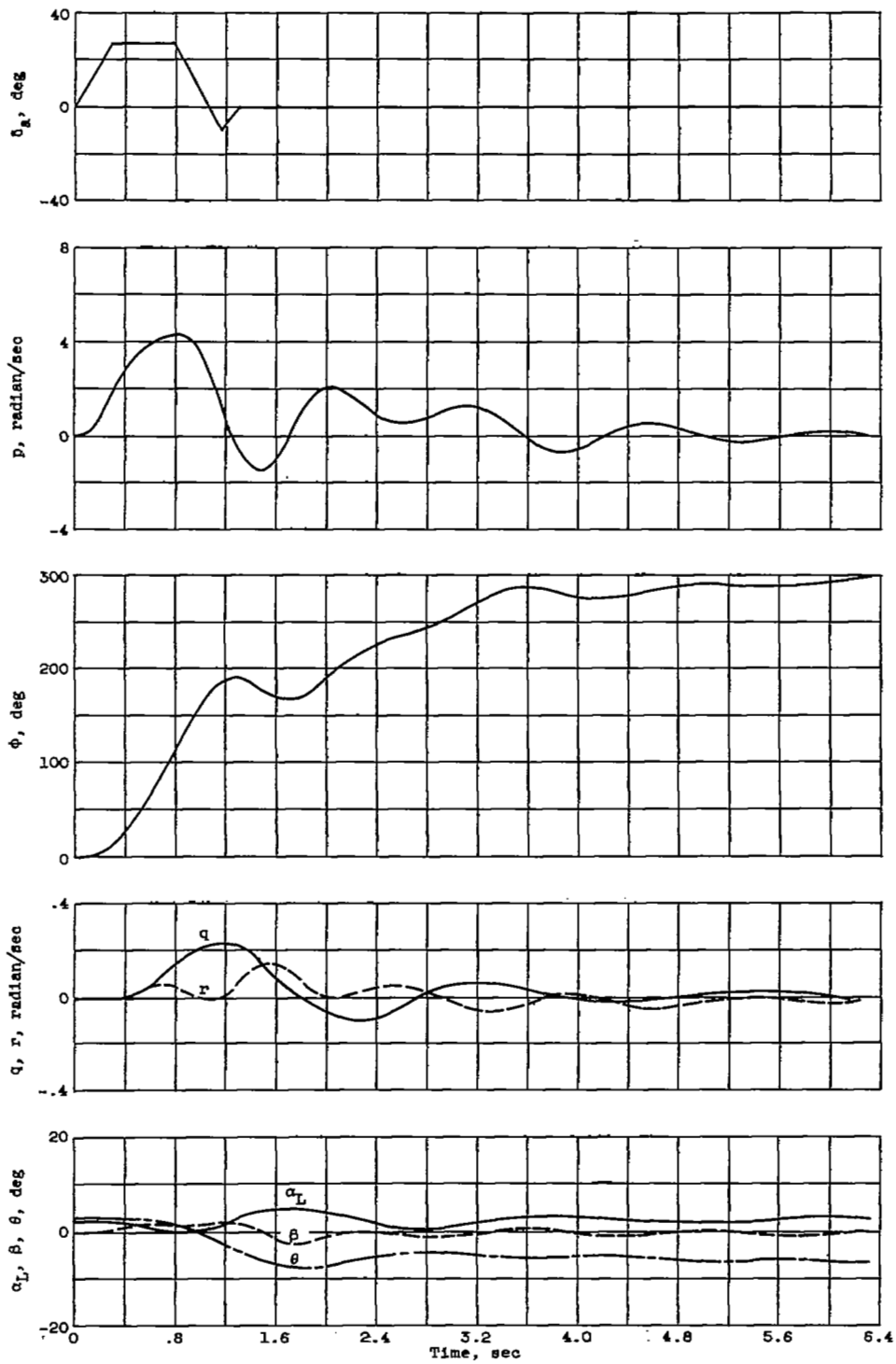

Figure 5. - Right-roll maneuver at Mach number of 1.5, altitude of 30,000 feet, and level flight. Rotor momentum included.

[redacted]

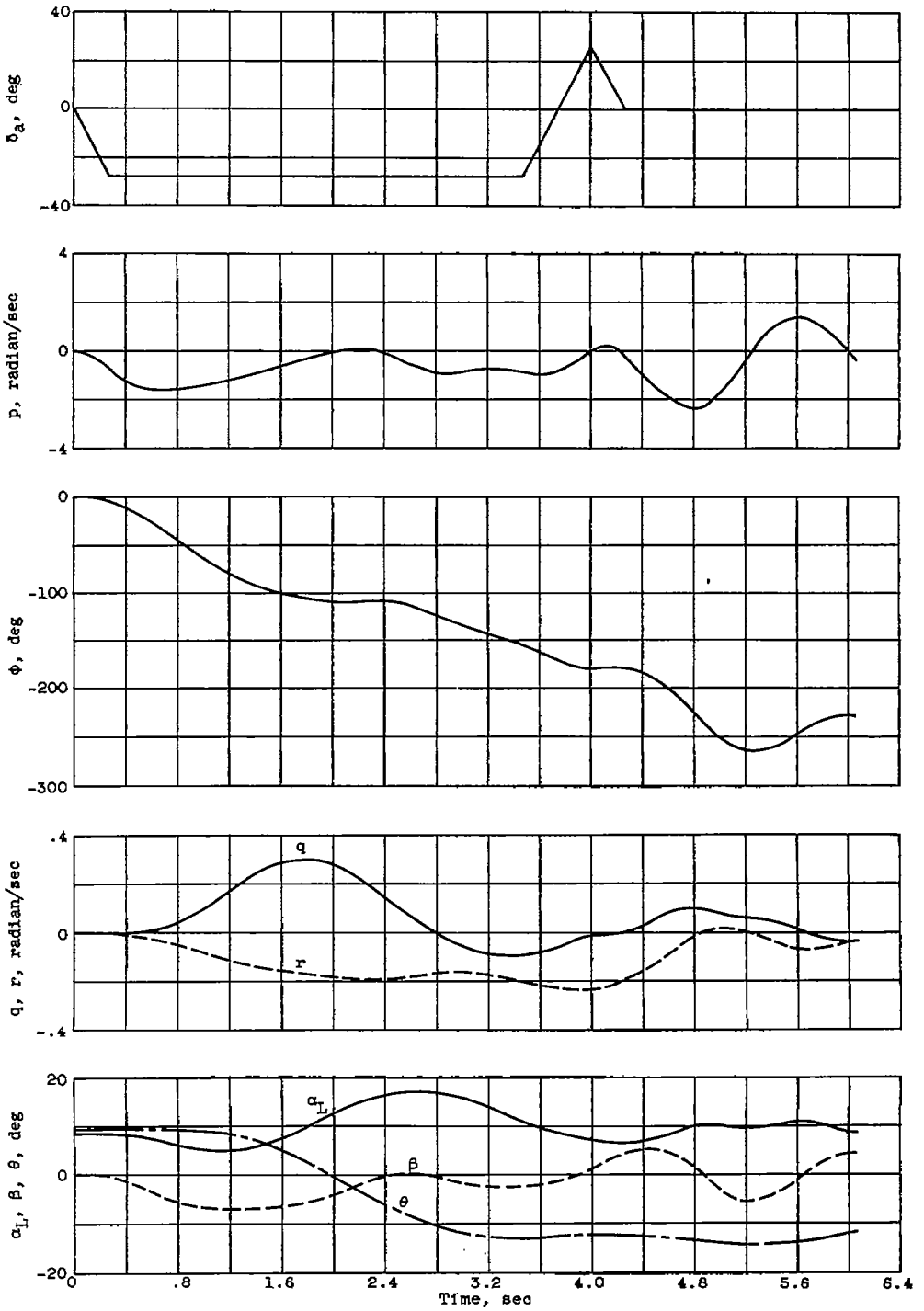

Figure 6. - Left-roll maneuver at Mach number of 1.5, altitude of 60,000 feet, and level flight.

[redacted]

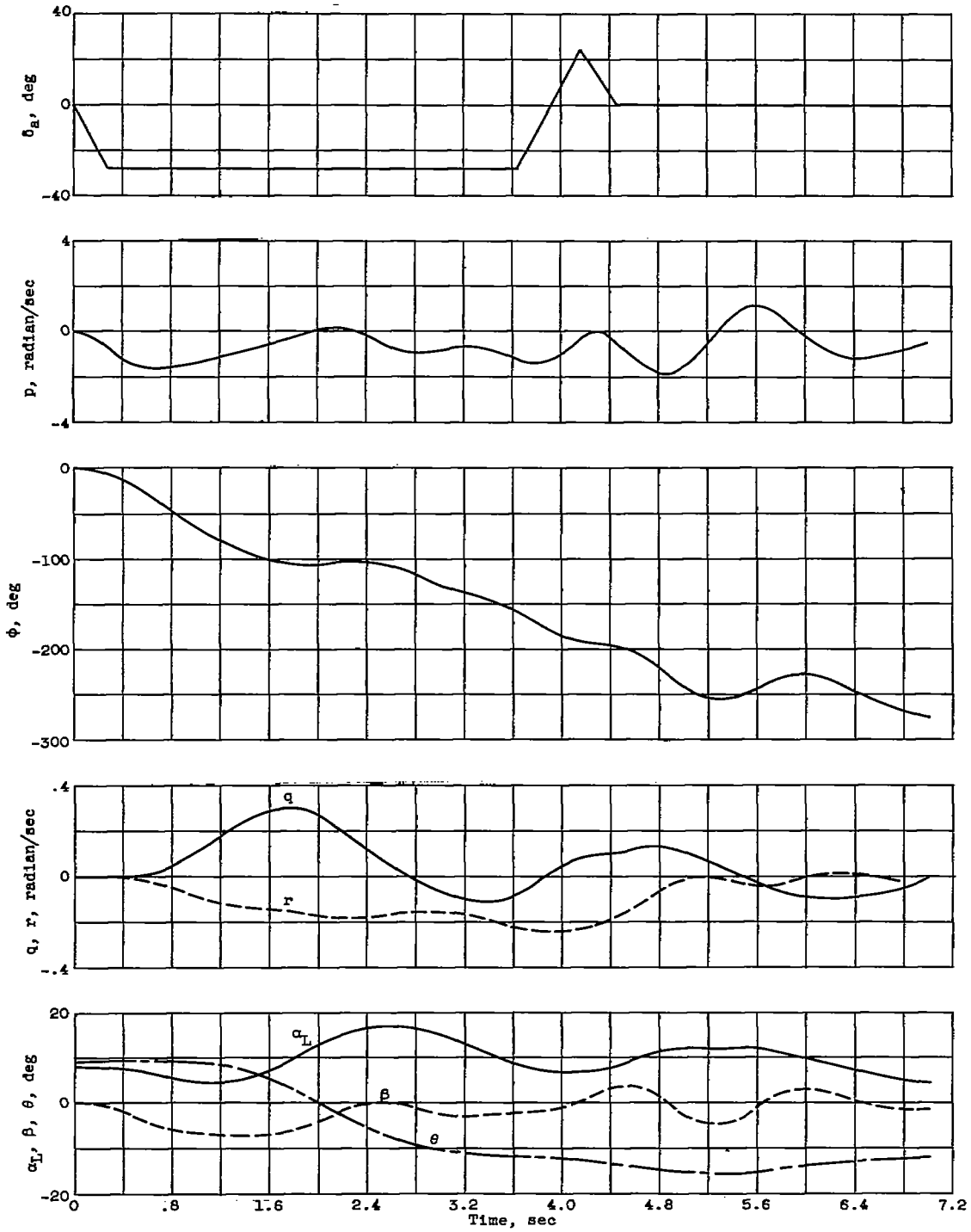

Figure 7. - Left-roll maneuver at Mach number of 1.5, altitude of 60,000 feet, and level flight. Rotor momentum included.

[redacted]

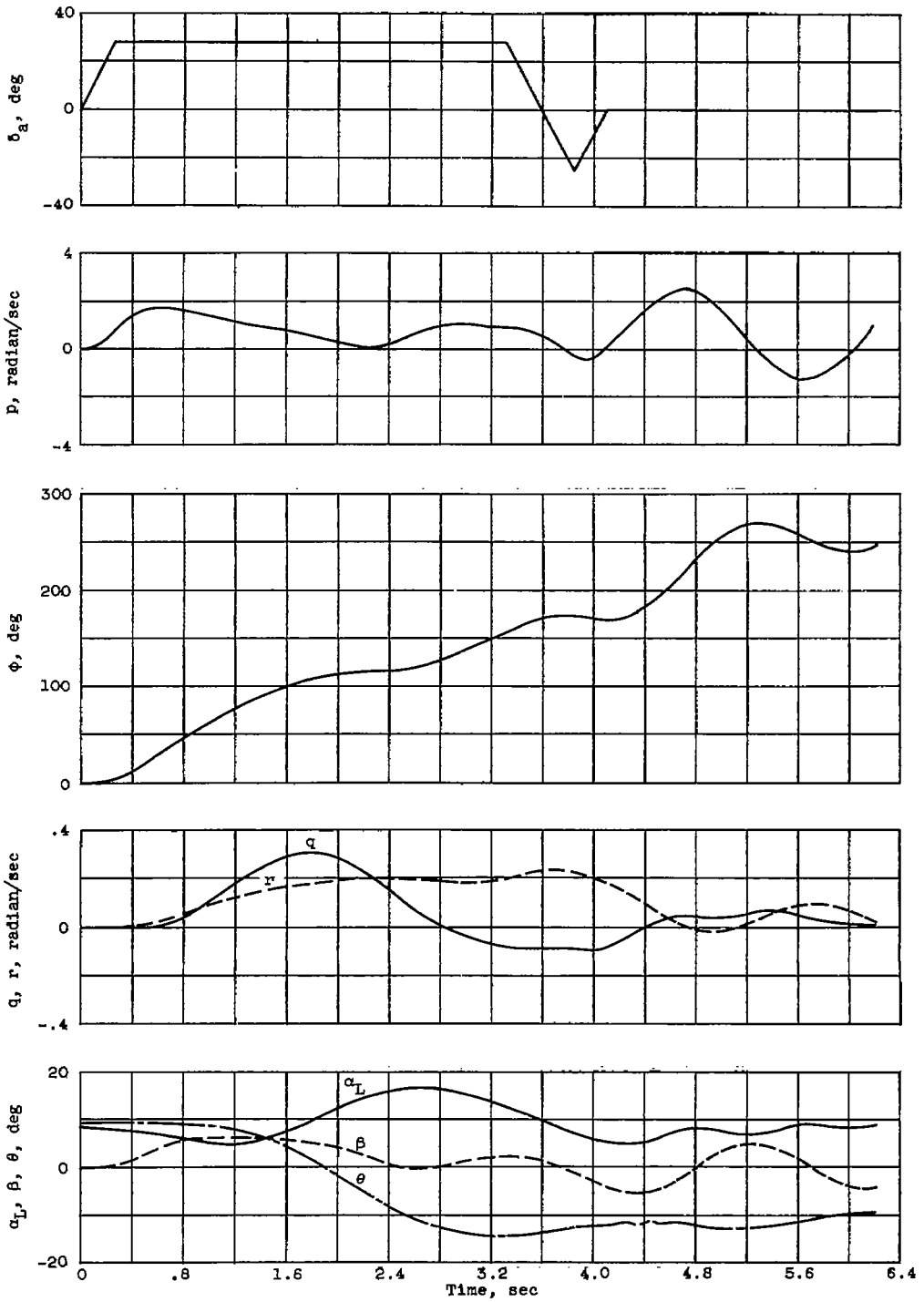

Figure 8. - Right-roll maneuver at Mach number of 1.5, altitude of 60,000 feet, and level flight. Rotor momentum included.

[redacted]

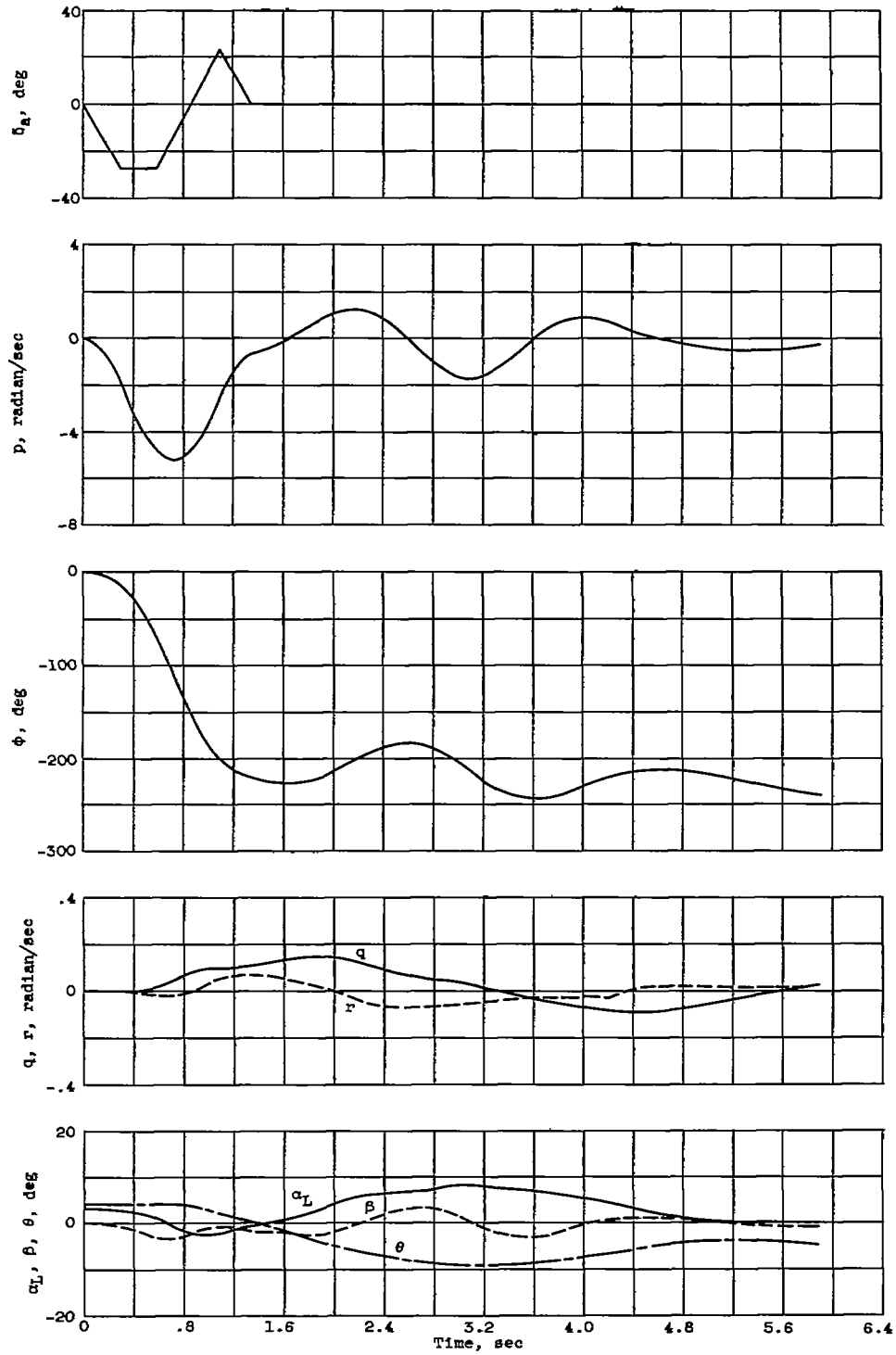

Figure 9. - Left-roll maneuver at Mach number of 3.5, altitude of 60,000 feet, and level flight.

[redacted]

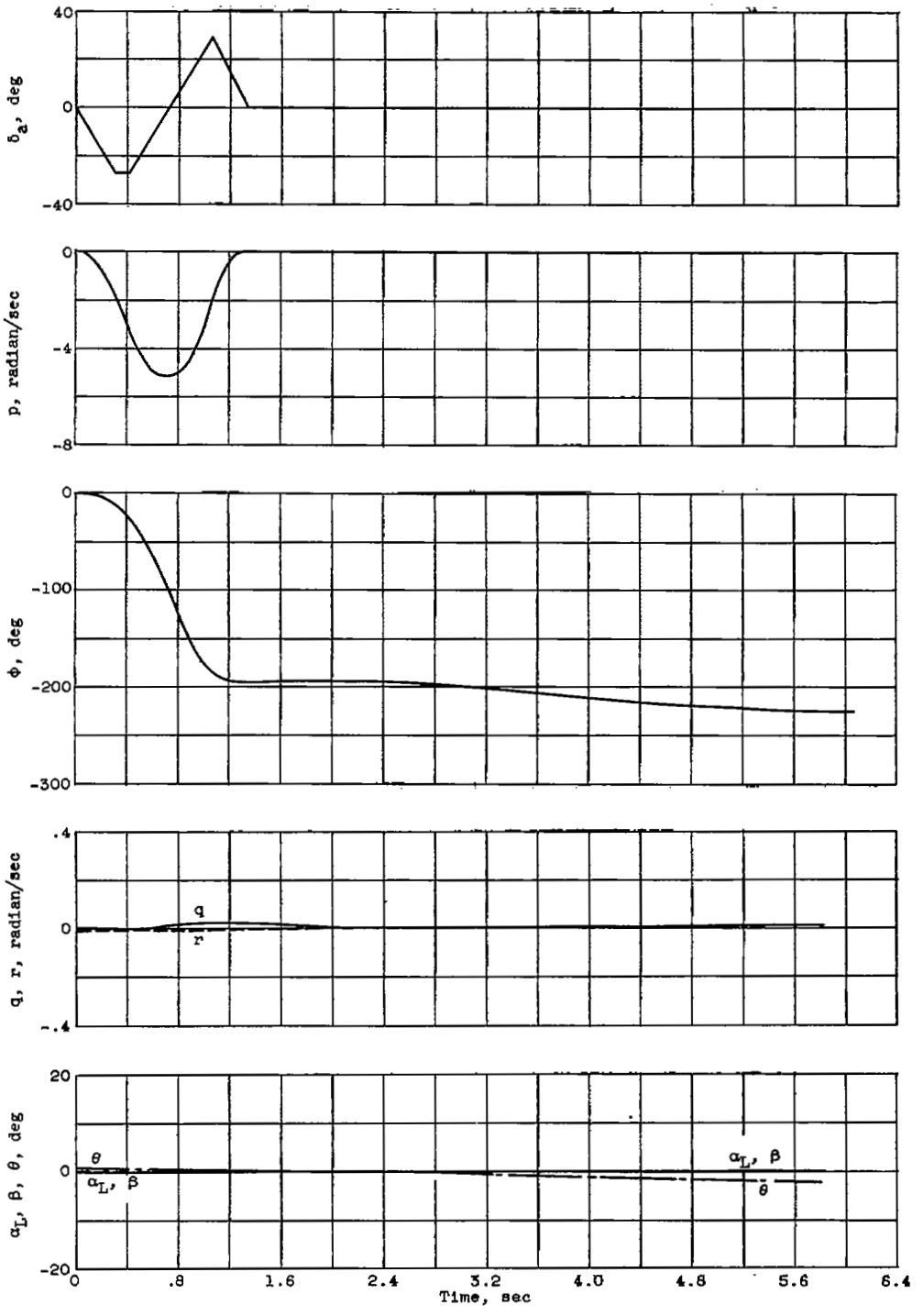

Figure 10. - Left-roll maneuver at Mach number of 3.5, altitude of 60,000 feet, and zero g pushover.

[redacted]

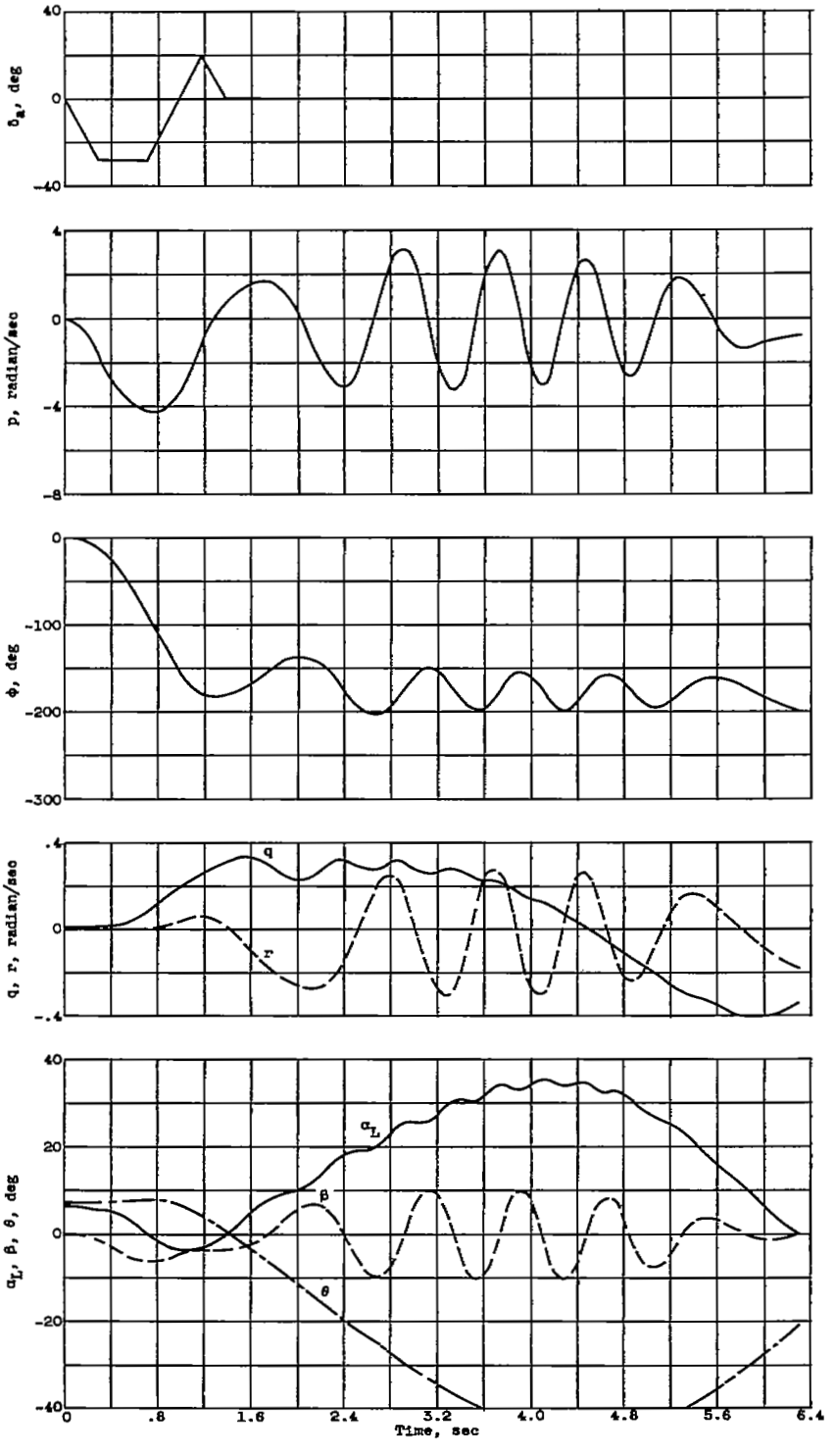

Figure 11. - Left-roll maneuver at Mach number of 3.5, altitude of 60,000 feet, and 2 g pull-up.

[redacted]

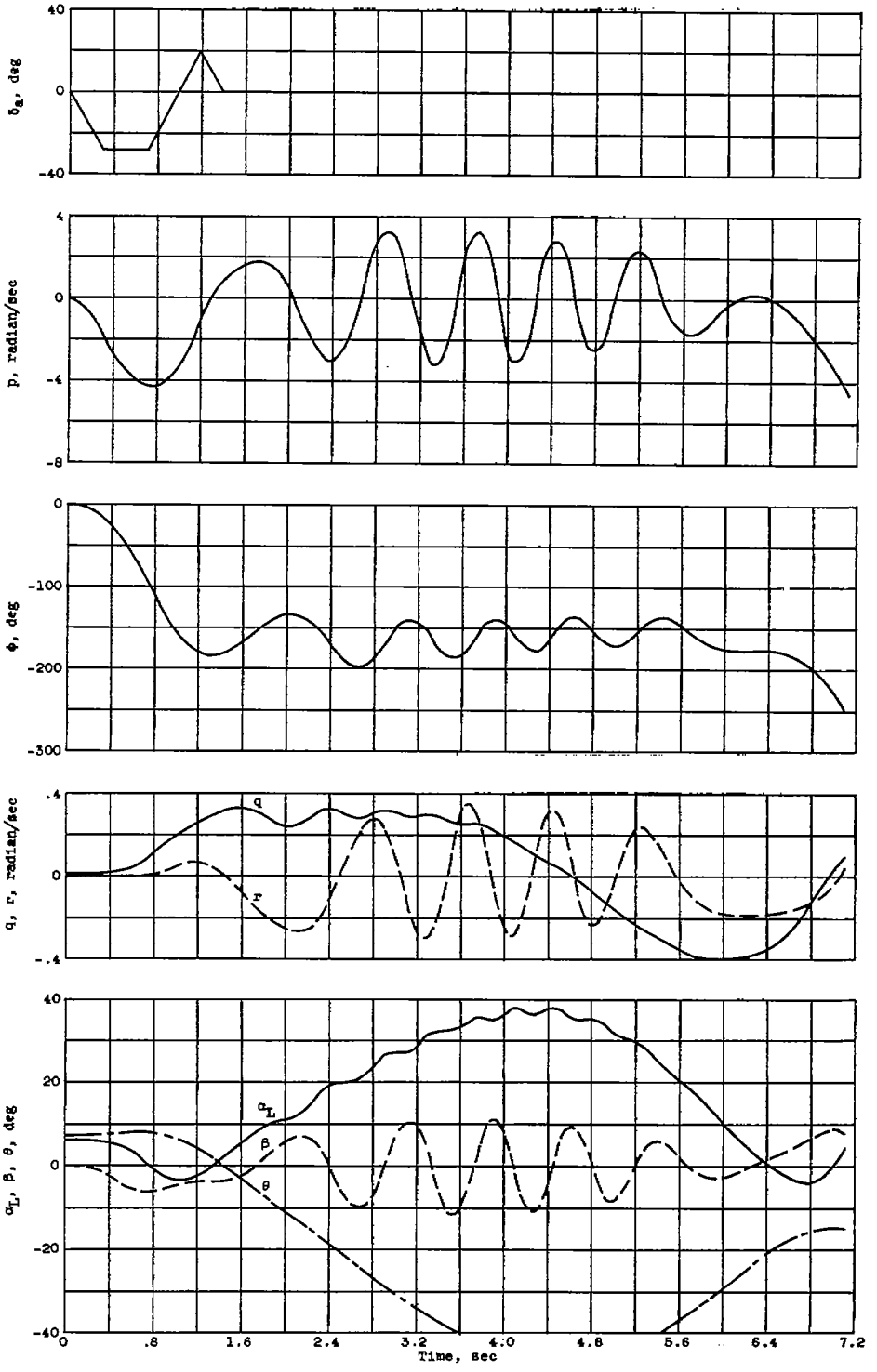

Figure 12. - Left-roll maneuver at Mach number of 3.5, altitude of 60,000 feet, and 2 g pull-up. Rotor momentum included.

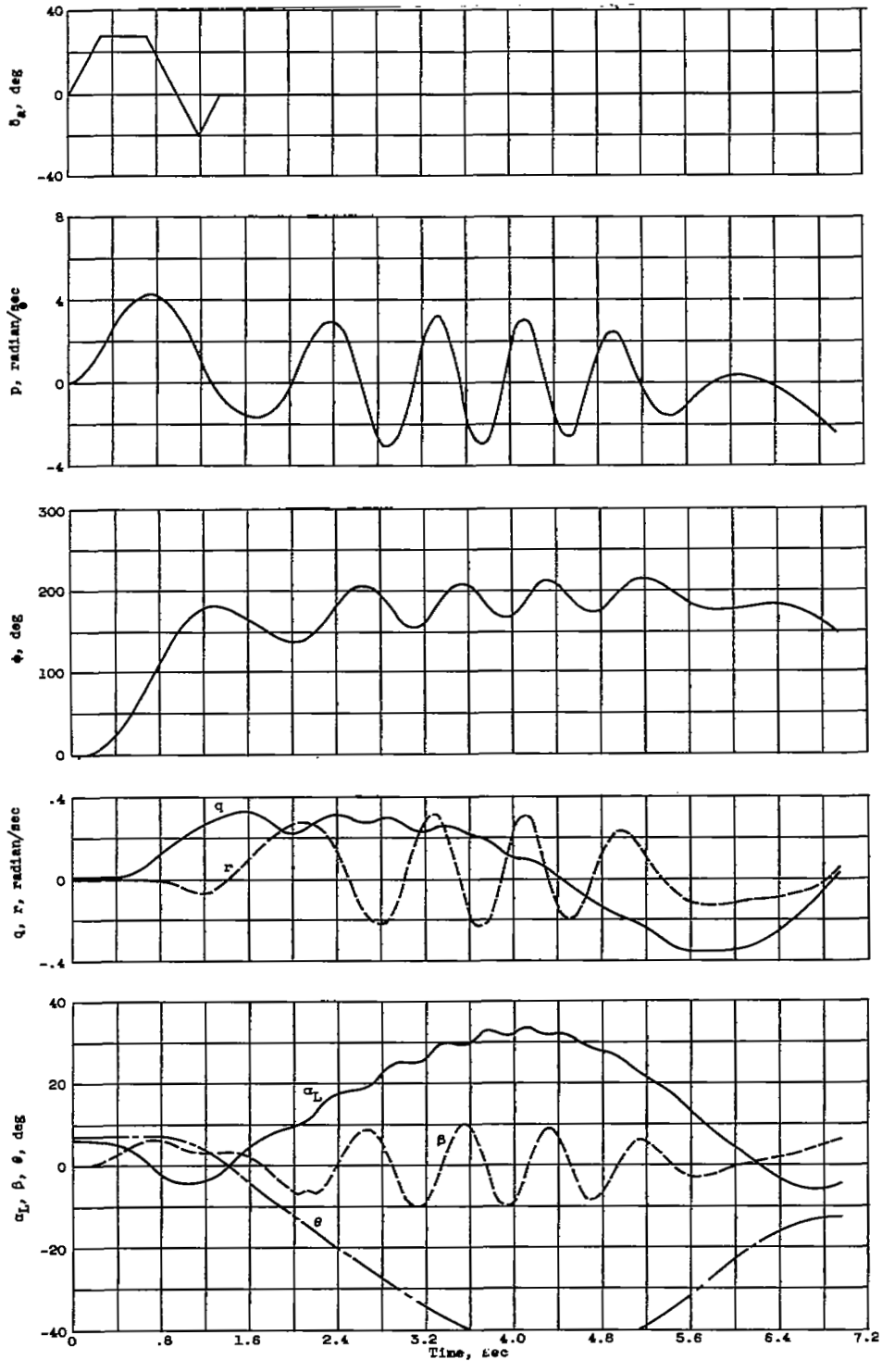

Figure 13. - Right-roll maneuver at Mach number of 3.5, altitude of 60,000 feet, and 2 g pull-up. Rotor momentum included.

[redacted]

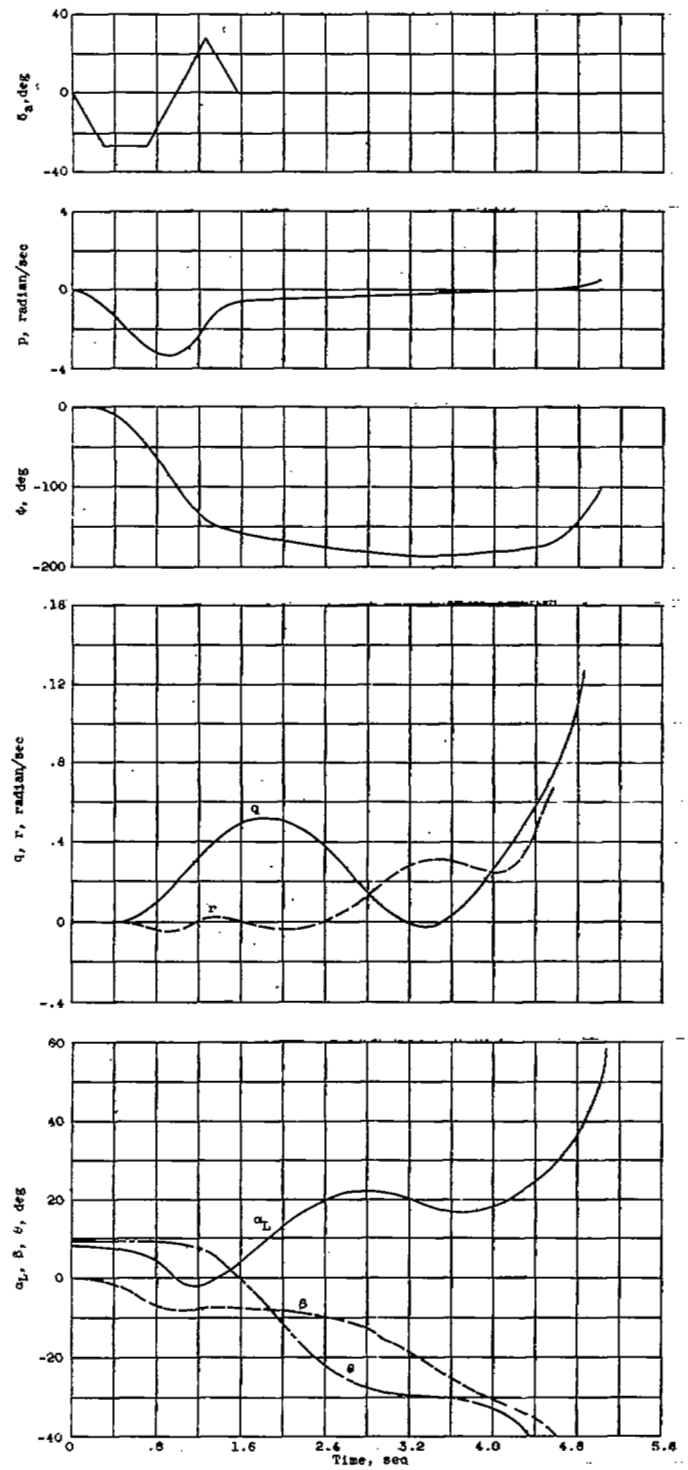

Figure 14. - Left-roll maneuver at Mach number of 1.5, altitude of 60,000 feet, and level flight. $C_{l_\beta} = 0$.

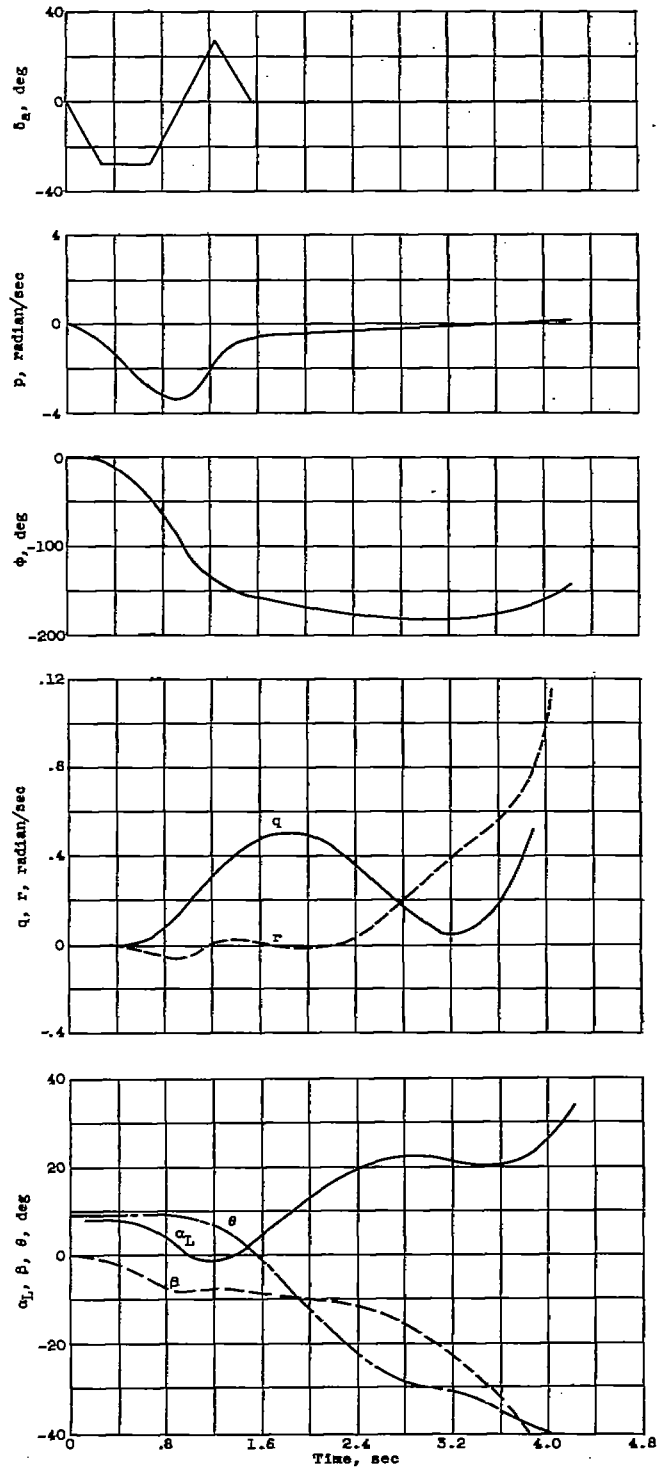

Figure 15. - Left-roll maneuver at Mach number of 1.5, altitude of 60,000 feet, and level flight. $C_{l_\beta} = 0$; rotor momentum included.

[redacted]

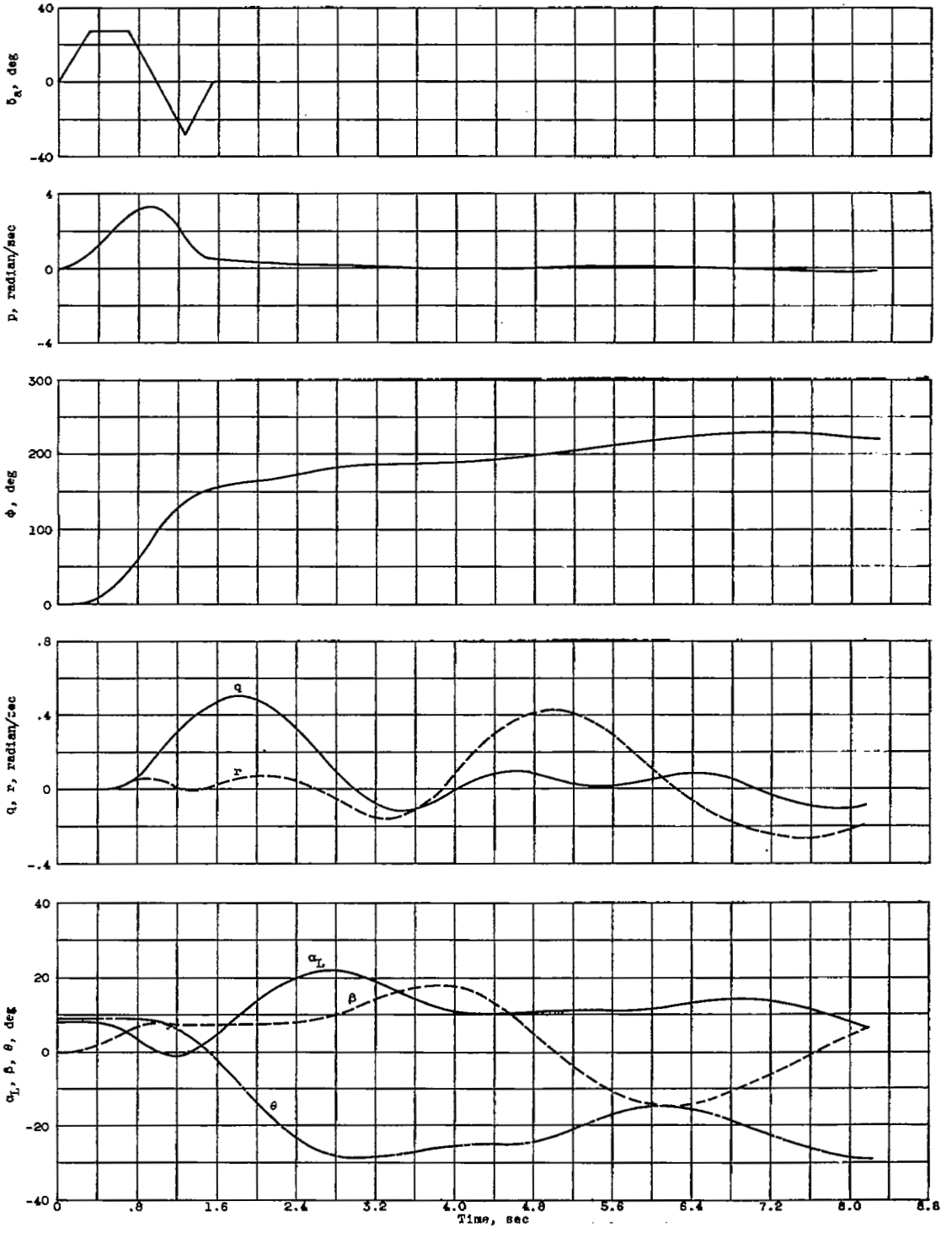

Figure 16. - Right-roll maneuver at Mach number of 1.5, altitude of 60,000 feet, and level flight. C_{l_β} = 0; rotor momentum included.

[redacted]

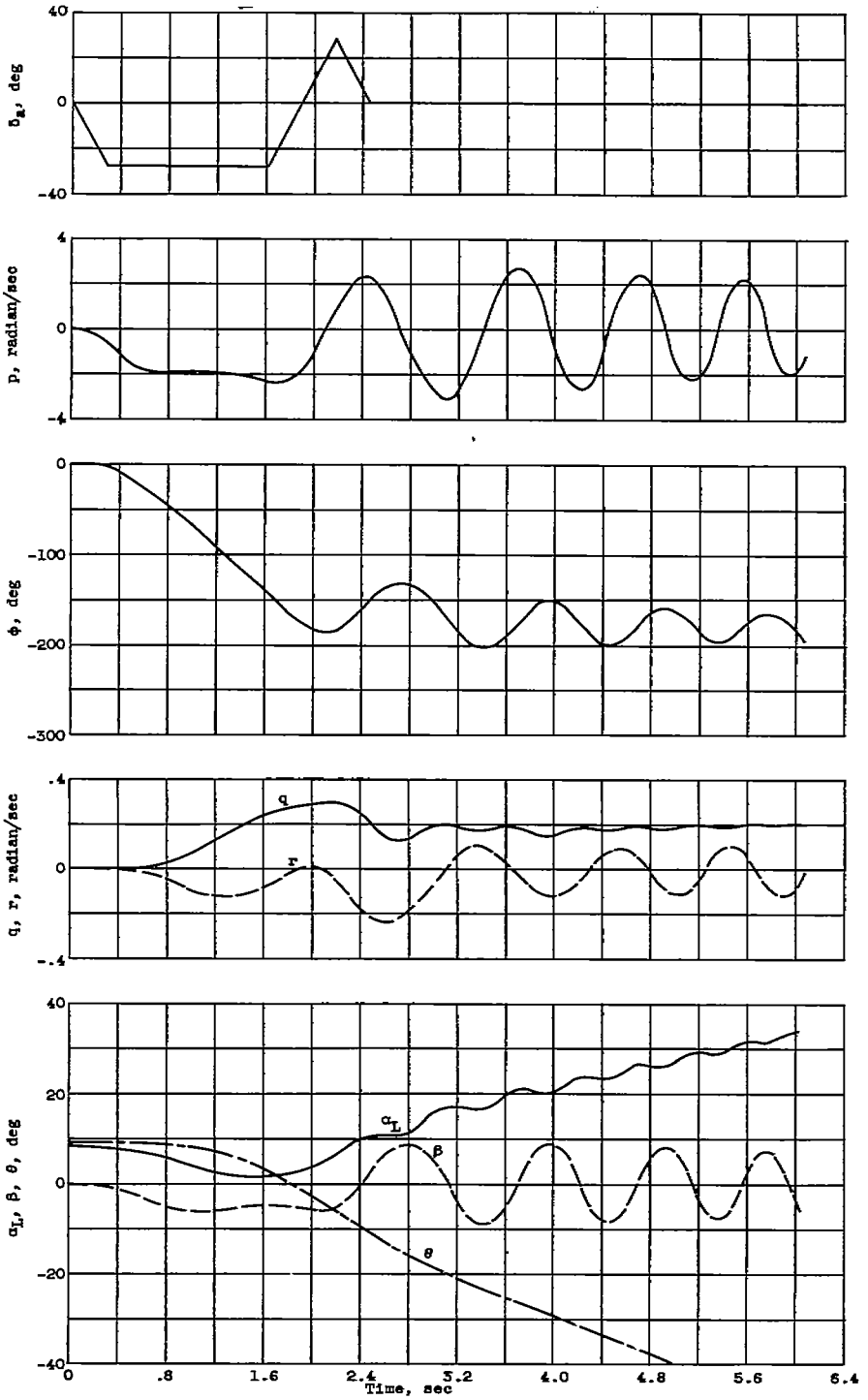

Figure 17. - Left-roll maneuver at Mach number of 1.5, altitude of 60,000 feet, and level flight. $C_{m_\alpha} = -0.00124$.

[redacted]

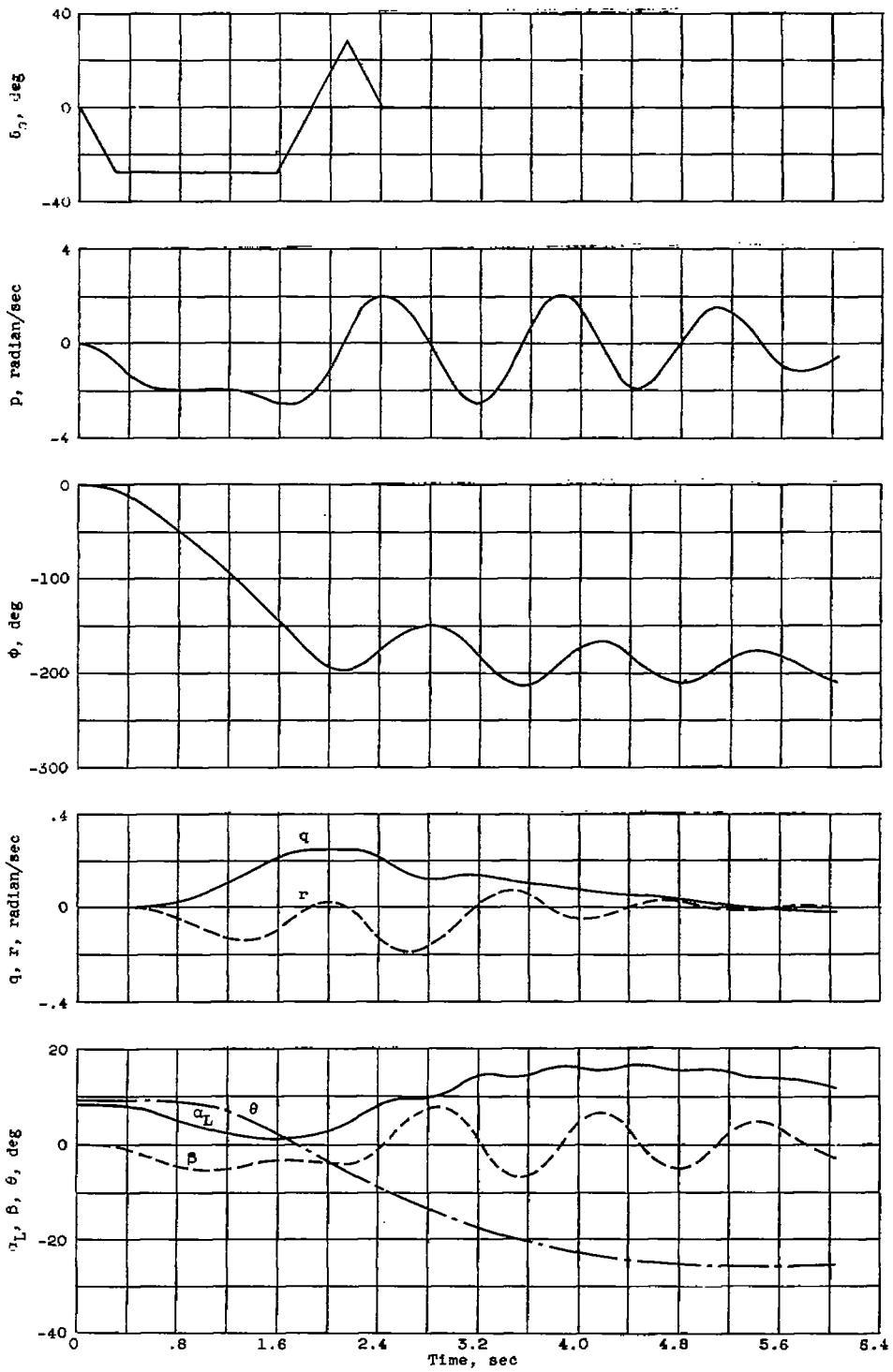

Figure 18. - Left-roll maneuver at Mach number of 1.5, altitude of 60,000 feet, and level flight. $C_{m_\alpha} = -0.00124$; $C_{m_{\beta 2}} = 0$.

[redacted]

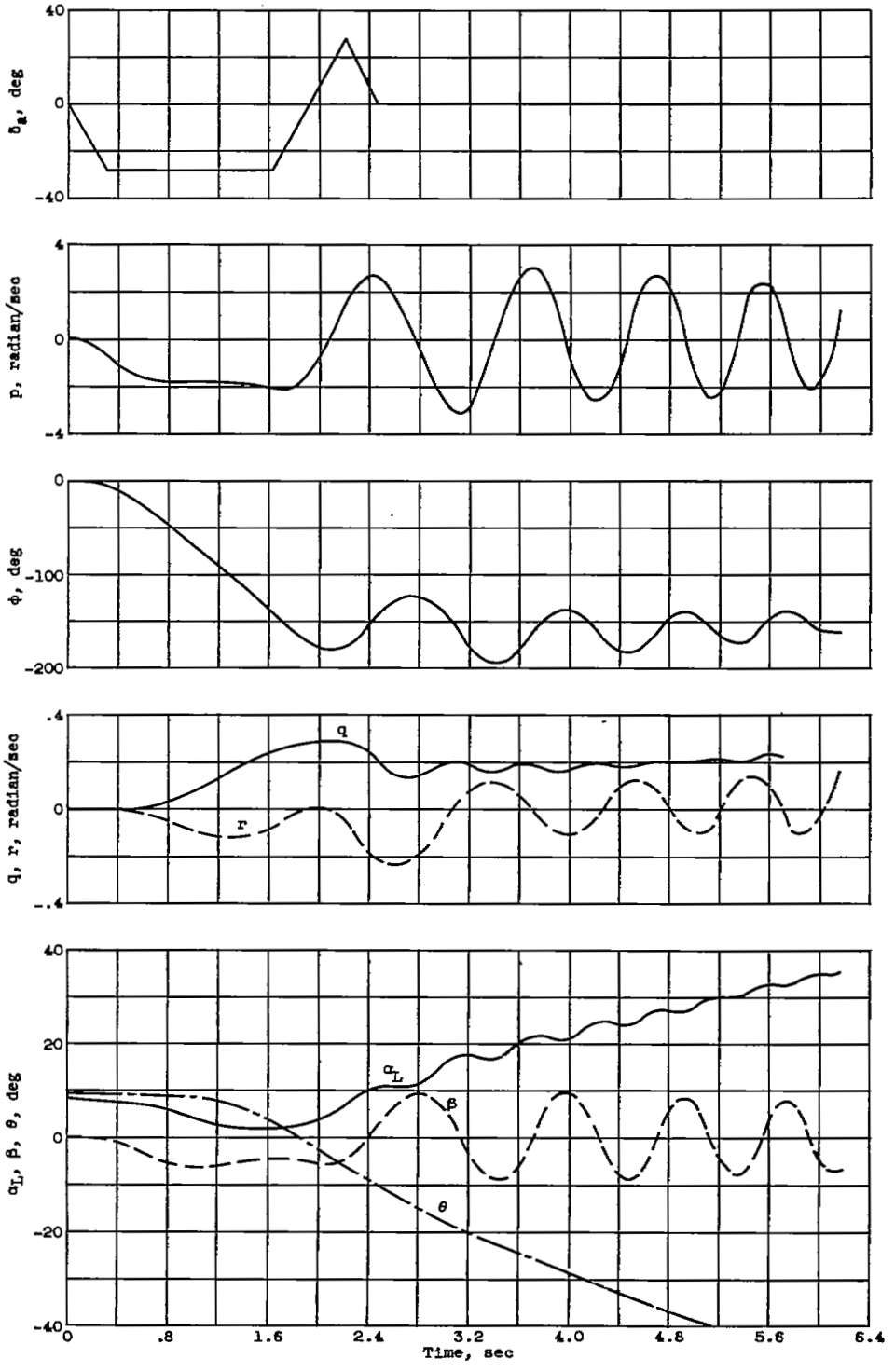

Figure 19. - Left-roll maneuver at Mach number of 1.5, altitude of 60,000 feet, and level flight. C_{m_α} = -0.00124; rotor momentum included.

[redacted]

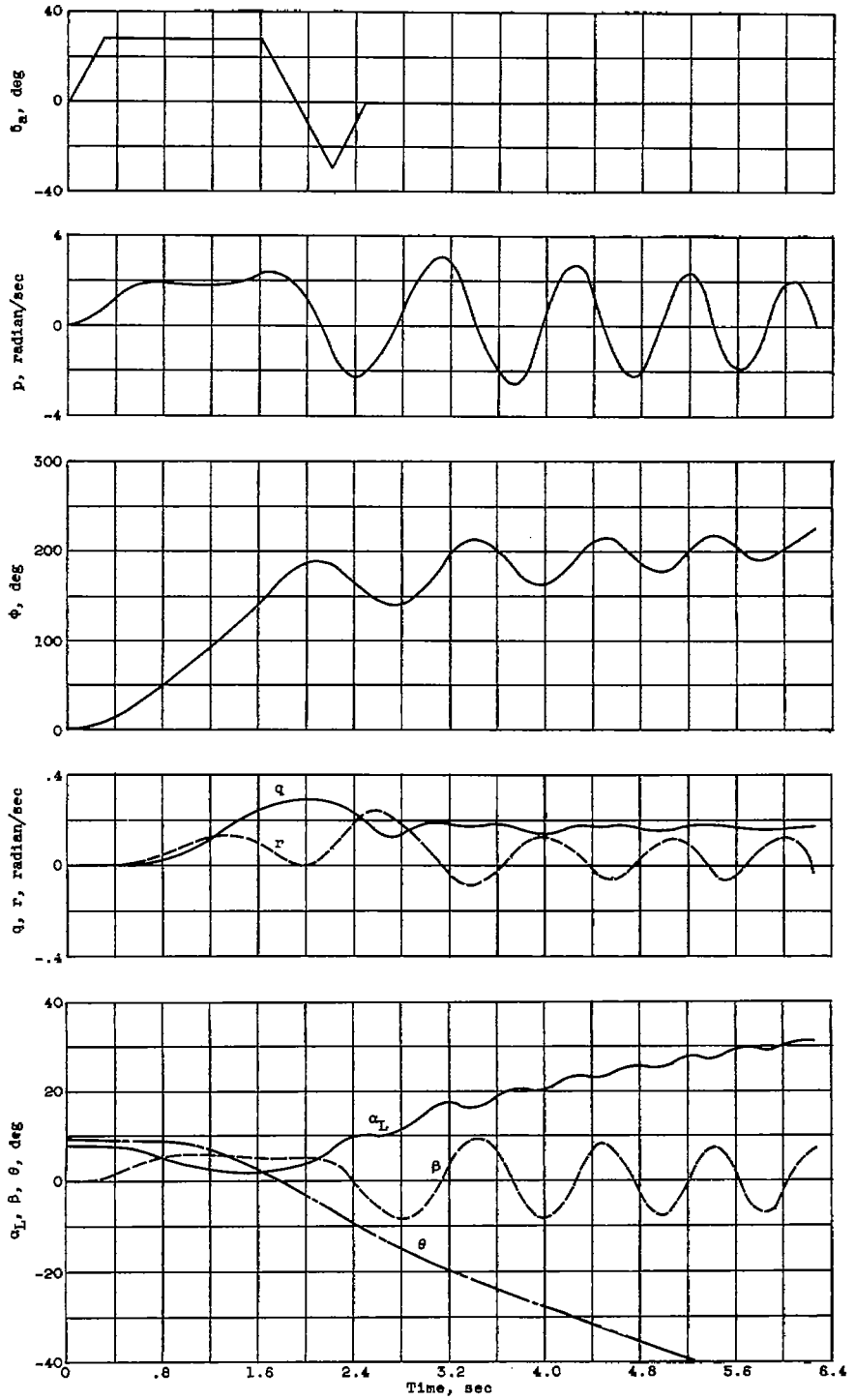

Figure 20. - Right-roll maneuver at Mach number of 1.5, altitude of 60,000 feet, and level flight. C_{m_α} = -0.00124; rotor momentum included.

[redacted]

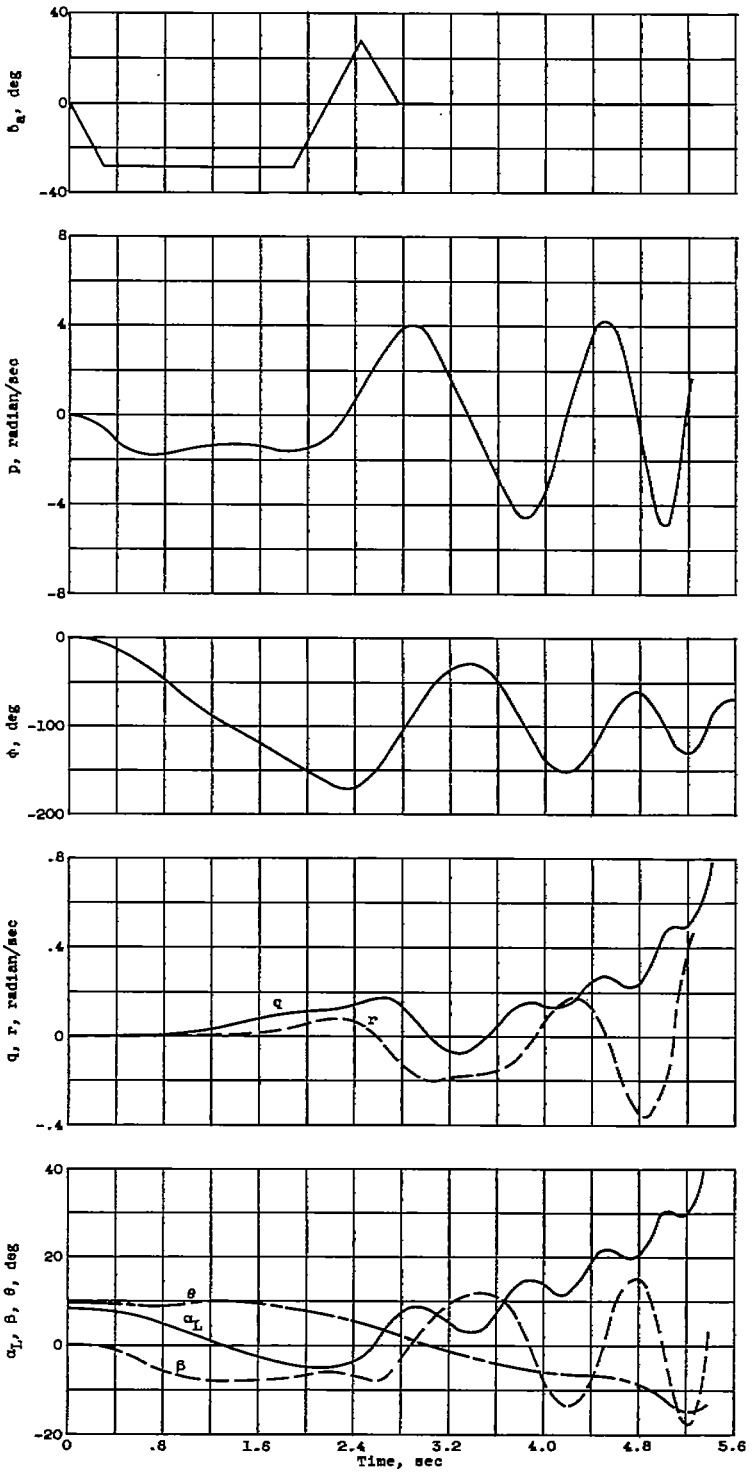

Figure 21. - Left-roll maneuver at Mach number of 1.5, altitude of 60,000 feet, and level flight. $C_{m_\alpha} = -0.00124$; $C_{n_\beta} = 0.000536 - 0.166 \times 10^{-4}\ \alpha_L^2$.

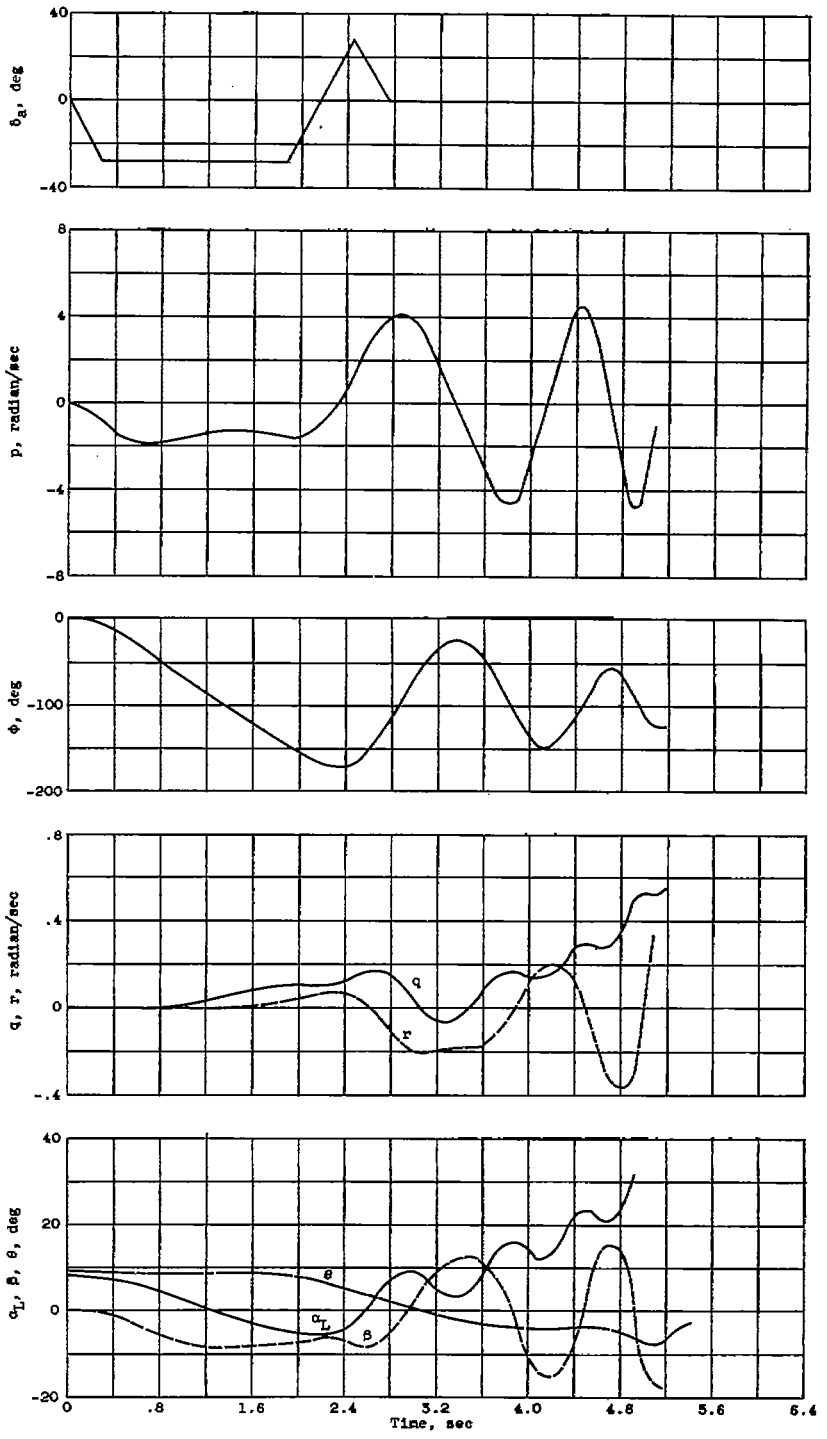

Figure 22. - Left-roll maneuver at Mach number of 1.5, altitude of 60,000 feet, and level flight. $C_{m_\alpha} = -0.00124$; $C_{n_\beta} = 0.000536 - 0.166 \times 10^{-4}\ \alpha_L^2$; rotor momentum included.

[redacted]

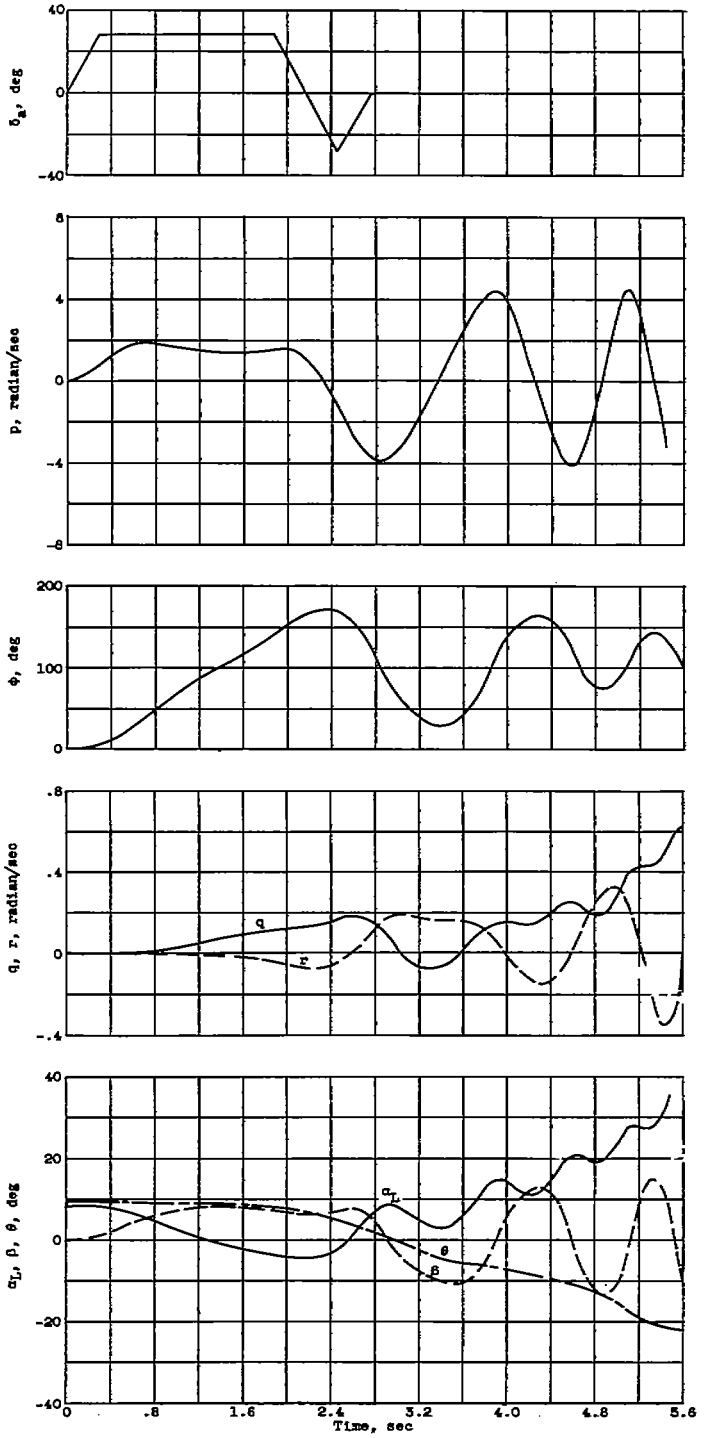

Figure 23. - Right-roll maneuver at Mach number of 1.5, altitude of 60,000 feet, and level flight. $C_{m_\alpha} = -0.00124$; $C_{n_\beta} = 0.000536 - 0.166 \times 10^4 \alpha_L^2$; rotor momentum included.

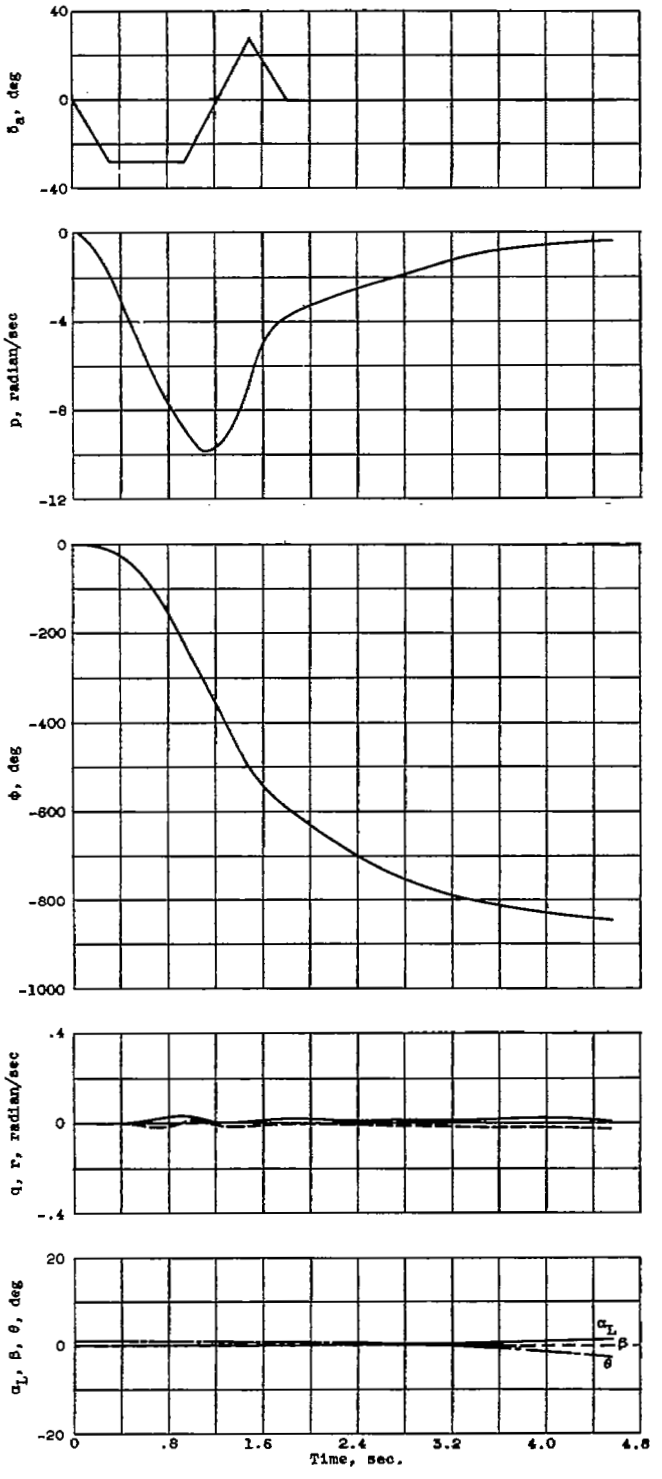

Figure 24. - Left-roll maneuver at Mach number of 3.5, altitude of 60,000 feet, zero g pushover, and large roll rate.

[redacted]

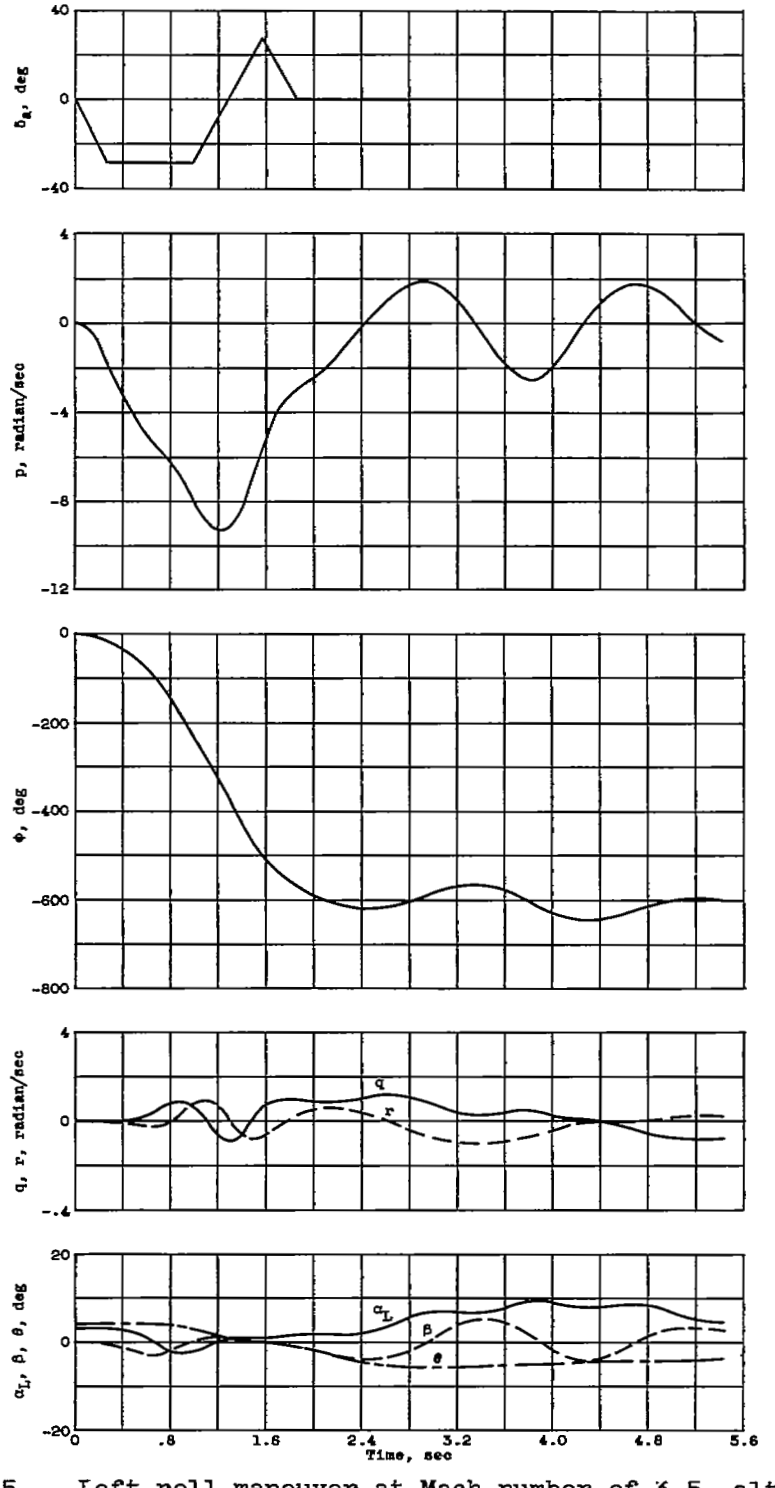

Figure 25. - Left-roll maneuver at Mach number of 3.5, altitude of 60,000 feet, level flight, and large roll rate.

[redacted]

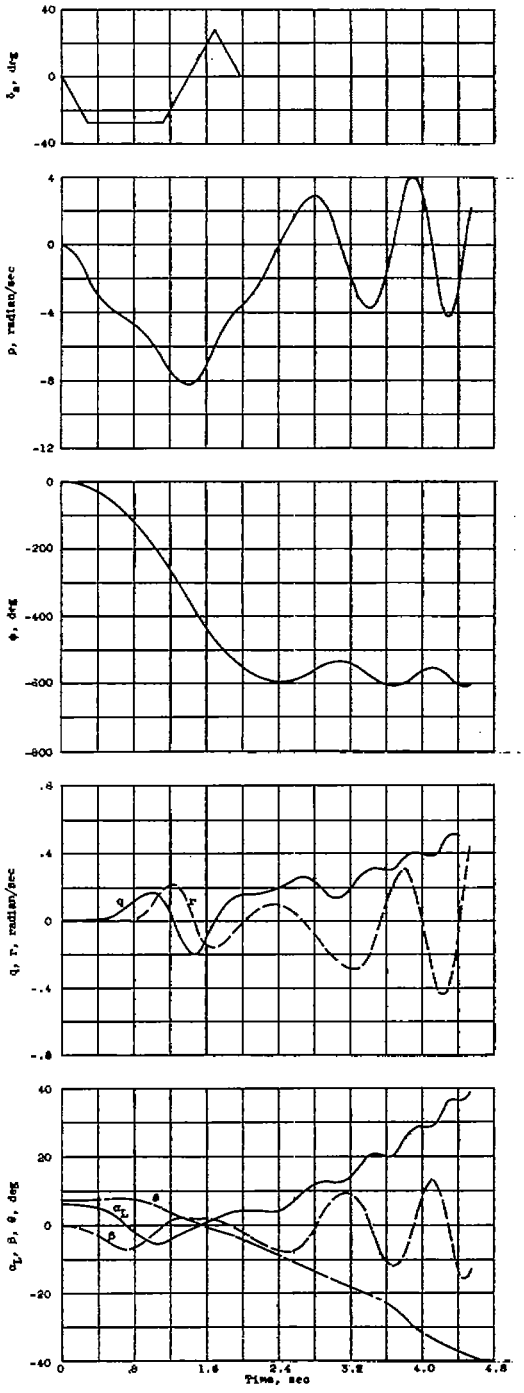

(a) Large roll rate.

Figure 26. - Left-roll maneuver at Mach number of 3.5, altitude of 60,000 feet, and 2 g pull-up.

[redacted]

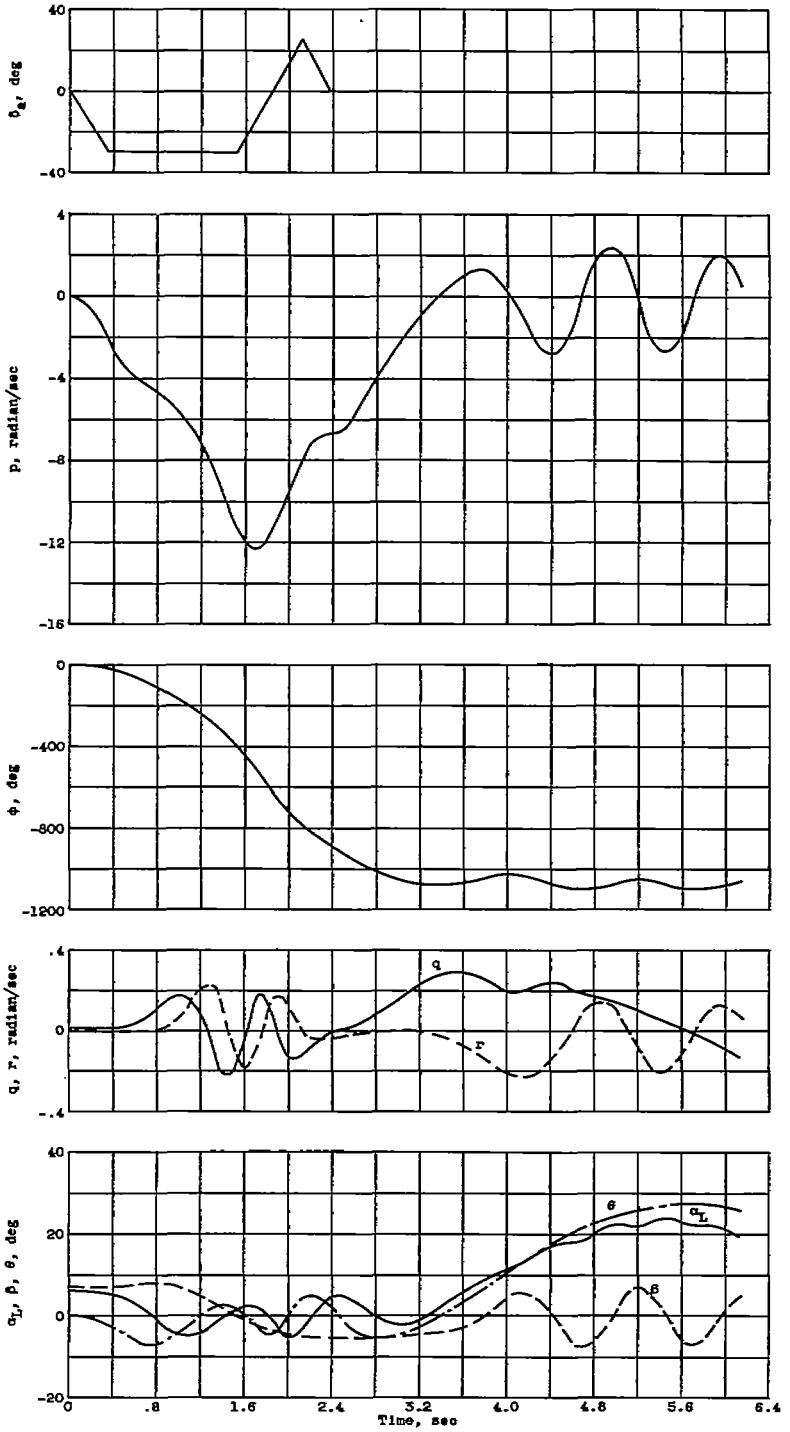

(b) Extreme roll rate.

Figure 26. - Concluded. Left-roll maneuver at Mach number of 3.5, altitude of 60,000 feet, and 2 g pull-up.

[redacted]